Spring 5-2019

Research of Electro-optical effect in Metal Halide Perovskites by Fabry-Perot interometer Method

Hanxiang Yin
Washington University in St. Louis

Washington University in St. Louis

McKelvey School of Engineering

Department of Mechanic Engineering and Material Science

Thesis Examination Committee:

Lan Yang, Chair

Kathrine Flores

Damena Agonafer

Research of Electro-optical effect in Metal Halide Perovskites by Fabry-Perot interometer Method

By

Hanxiang Yin

A thesis presented to the McKelvey School of Engineering of Washington University in St. Louis in partial fulfillment of the requirements for the degree of Master of Science

2019 May

St. Louis, Missouri

Acknowledgements

First and foremost, I would like to show my deepest gratitude to my supervisor, Dr. Yang Lan, a respectable, responsible and resourceful scholar, who has provided me with valuable guidance in every stage of the writing of this thesis. Without her enlightening instruction, impressive kindness and patience, I could not have completed my thesis. Her keen and vigorous academic observation enlightens me not only in this thesis but also in my future study.

I shall extend my thanks to Dr. Huang Su for all his kindness and help. I would like to thank him for helping me develop the fundamental and essential academic competence. My sincere appreciation also goes to the teachers and students from the group, including Linhua Xu, Yihang Li, Changqing Wang, who gave me help in experiment and literature searching.

Table of Contents

List of Tables

List of Figures

Abstract

By

Hanxiang Yin

Master of Science in Material Science

Washington University in St. Louis, 2019

Research Advisor: Professor Lan Yang

Organometal halide perovskites materials has been popular for its outstanding optoelectronic properties and the excellent performance in solar cell and photovoltaic applications. This thesis mainly pays attention to electro-optic (EO) effect of organometal halide perovskites for the potential in semiconductor industry in related second harmonic generation.

Methylamonium lead iodide ($CH_3NH_3PbI_3$, or called $MAPbI_3$ in short) is chosen as the material for study because previous studies have proved its ability of forming film with high optical property by spin-coating. This thesis uses Fabry-Perot method to measure the EO coefficient in $MAPbI_3$, which has been used for measurement of the EO coefficient of other kinds of perovskites. Different from them, the data of transmission ratio is used in the analysis of the properties rather than reflection in this project.

In the first part of this thesis, details of the fabrication of the Fabry-Perot interferometer containing $MAPbI_3$ are discussed in order to get ideal conditions for following experiments. Then transmission signals of 1550 nm laser are collected from the lock-in amplifier connected to

samples. Calculation of the EO coefficients from these data helps us figure out the details of EO properties of $MAPbI_3$ and leave data which is also useful for further studies.

Chapter 1 Introduction

In this project, I used the method of prepare one Fabry-Perot interferometer containing halide perovskite and characterize the response when electric field is applied to it in order to calculate the constant of electro-optical effect. Before the part of experiment and analysis of the data, basic theories related to this project need to be introduced as the preparation.

Background Information from Previous Researches

In 1839, scientists E. Becquerel found the photovoltaic situation of liquid in France. Over the following, 100 years scientists studied the photovoltaic effect of various kinds of metal, their sulfide and oxide including copper, selenium and cadmium. In 1941, photovoltaic effect was found on silicon and then the first solar cell made of monocrystalline silicon appeared in Bell laboratory in 1954. As time goes on, the efficiency of silicon solar cell was rapidly improved and polycrystalline silicon displaced monocrystalline silicon in industry gradually because of its convenience in cost and technology. However, Matsushita made great breakthrough in the efficiency limit in Japan in 2003 and developed advanced technology like heterojunction monocrystalline, backcontact monocrystalline, diamond line slicing, monocrystalline back passivation and monocrystalline straight pulling furnace, which made the cost of monocrystalline silicon industry no larger than polycrystalline silicon and helped monocrystalline silicon achieved the dominant role in modern industry because of the advantage in its higher efficiency and longer lifetime.

Over the past ten years, researchers have made extraordinary progress in improving the efficiency of monocrystalline silicon in circuit elements and finally got closer to the theoretic limit of monocrystalline silicon. As a result, studies of other kinds of material with better electronic properties. Reports of the second generation of semiconductors have been made in late

1990s, along with the beginning of the study of monocrystalline silicon. However, the requirement of better material for semiconductor promotes the study of the second and third generation of semiconductor, leading to the development of different kinds of semiconductor materials like germanium, gallium and indium. With the rapid development of electronic industry in the 21st century, researchers have paid attention more than metal, alloy and their oxide and started to focus on more crystals with complex structures and more elements. Ceramics, processed inorganic materials, have been be far made and used in the highest volume and weight by humankind. Ceramics have tens of thousands of crystal structures, but only half a dozen specific ceramic phases dominate the application of these material in industry, not only in terms of volume, weight and other fundamental advantages, but also in terms of technological significance, including quartz, mullite, calcium silicates, Al_2O_3 and TiO_2[1]. Most composites of these ceramic phases are useful because they have more than one important property valuable to the electronic industry. Yet there is still a question that they are mostly made of two elements. Could some ternary structures be found to have similar photoelectronic properties? After examinations of a list of ternary structures, the data reveals that among thousands of structures, the A_2BX_4 structure, spinel, and the ABX_3 structure, perovskite, are really outstanding, while perovskite is far ahead of spinel since materials in the former structure can appear a list of totally different functions with different composition.

Introduction of Perovskites

Oxide Perovskite

The word ‘perovskite’ is first used for the name of a particular mineral with the composition $CaTiO_3$, and then gradually becomes the name of a structural family with the discovery of more and more minerals in the same structure and different composition and properties. At the

beginning, most studies were related to the origin mineral, $CaTiO_3$, and researchers mainly chose composites with the ligands of oxygen anion. Now as the typical structure has been well studied, a wide array of composites have been achieved by changing the cation and central ion and researched for their properties in various areas which indicate a lot of potential applications.

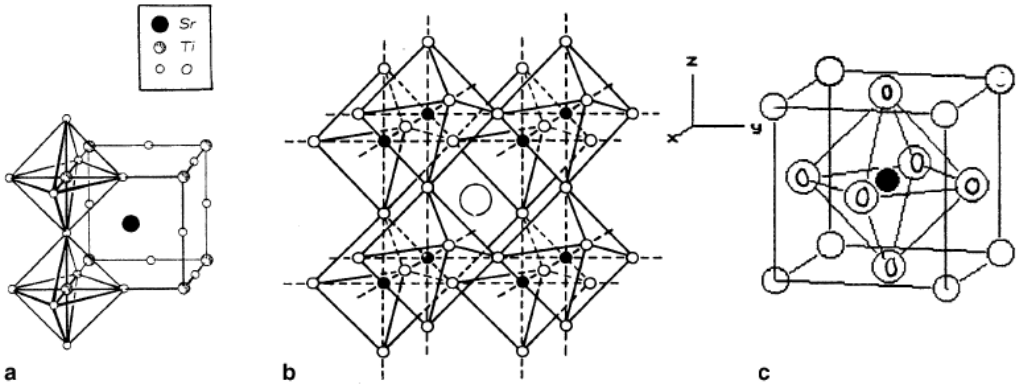

Figure 1 Fundamental crystal structure of perovskites

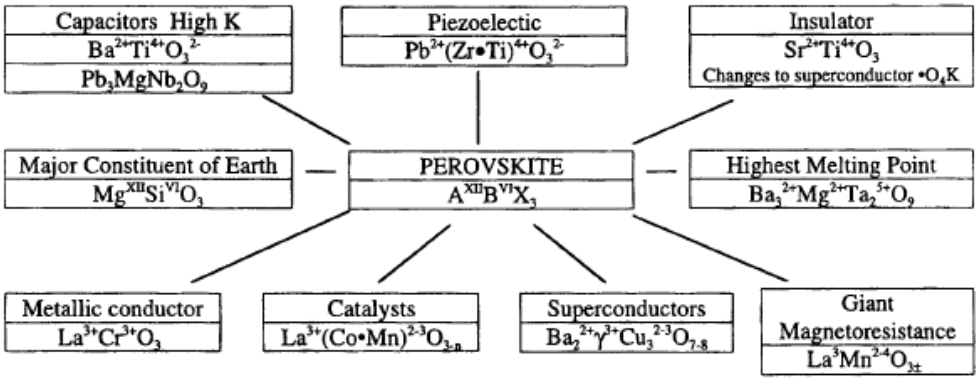

Figure 2 Existing and potential applications of perovskite

The first useful property found in perovskite is the high dielectric constant in $BaTiO_3$. During the World War II, the demand of substitute of muscovite mica, $KMg_3(AlSi_3)O_{10}(OH)_2$, which is the key insulator in most capacitors and crucial to skyrocketing, is urgent because of the loss of supply line. Researchers in Cleverland, Moscow and Tokyo identified $BaTiO_3$ as the one

they required at almost the same time[2-5]. Further studies by 1950 started to pay more attention to its optical domain and more related electronic properties and reported two important properties, ferroelectricity and superconductivity[6-10], which finally led to the wide application of perovskite more than just $BaTiO_3$ in the industry of electroceramics.

Table 1 Major applications of most ferroic perovskites

Ferroic perovskites	Major applications
$BaTiO_3$	Capacitors
$PbTiO_3$	Pyroelectric detectors
$Pb(Zr_{1-x}Ti_x)O_3$	Piezoelectric components
$PbLa(ZrTi)O_3$	Transparent inorganic materials, electrooptic tools
$LiNbO_3$	Optical modulators
$LiTaO_3$	Pyroelectric sensors
$KNbO_3$	Second harmonic generators
$Ba_xRh_{1-x}TiO_3$, $K_xRh_{1-x}TiO_3$	Photorefractive material
$SrTiO_3$	Tunable microwave material

Hailde Perovskites

By 2019, various properties related to the ferroelecticity and superconductivity of the oxide perovskite, with the chemical formula of ABO_3, have been analyzed from results of experiments of artificial crystal in the laboratory. However, another kind of perovskite has attracted the public attention for its outstanding performance in solar cells and other photoelectrical devices, with the name of halide perovskite. Metal halide perovskites, usually described by ABX_3 (where A is a cation, B is a divalent metal cation and X is a helogen anion), are a class of semiconductors of

great potential in optical and electronic properties. In the early 1990s, field-effect transistors (FETs) and light-emitting fiodes (LEDs) made from crystal organometal halide perovskites were firstly reported to own extraordinary optoelectronic properties by Mitzi and his coworkers[11,12,13,14,15]. During the past ten years, metal halide perovskites have been widely investigated for the unique electronic and optical properties which is potential to fields like advanced solar-to-fuel conversion devices, LED of high efficiency and photovoltaics. In 2009, a kind of hybrid organic-inorganic lead halide perovskite, $CH_3NH_3PbI_3$ which is often called $MAPbI_3$ for short (MA=methylamonium) was employed in liquid-electrolyte-based-dye-sensitized solar cells by Miyasaka and coworker in 2009[16]. Although the corrosion caused by the iodine redox from the liquid electrolyte led to a low conversion efficiency of only 3.8%, in following researches, the introduction of one new organic hole-transparent material replaced liquid electrolytes and appreciably raise the efficiency to 9.1%[17], quickly increasing to 20.1% in only two years[18,19,20]. Just following the breakthrough of solar cells, the studies concerned with the optoelectronic properties[21,22], capability of forming large single crystal with few defects[23] and low dimensional crystal with specific morphologies[24,25,26] led to new research interests in the fabrication of LEDs and photodetectors[27,28,29]. Researchers have realized low-cost LED with high luminance of 417cd/m^2 at room temperature[30], photodetector with the detectivity up to 10^{14} Jones, a linear dynamic range of 100 dB and the photoresponse of almost 3 MHz with 3 dB bandwidth made of halide perovskite[31] and $MAPbX_3$-contained wavelength-tunable nanowire lasing at low temperature with small threshold and high quality factor[32.] Researches by present have proved the value of halide perovskite in optoelectronic industry and the potential of more applications.

Introduction of Electro-optical Effect

After the invention of laser devices in 1960s, extensive study of intense coherent light and related fields. For materials research, one important study direction is the nonlinear optics. Nonlinear optics have been investigated and applied for optoelectronic components in modern industry.

Table 2 Compare of linear optics and non-linear optics

Linear optics	Nonlinear optics
No energy exchange between light and media and no change in the frequency of the light in propagation.	Interaction of light and media can change the frequency (frequency-doubled laser) and periodic spectrum distribution (simulated Raman scattering)
No energy exchange between different lights and no change of frequency	Energy exchange between lights can change the original frequency and produce new frequency (three-wave and four-wave mixing)
No change of physical properties of media caused by interaction with light	Physical properties like polarizability, absorption constant and refractive index are determined by the strength of field (nonlinear absorption and dispersion, Kerr effect, autofocusing)
Strength of transmit light in linear to incident light	Strength of transmit light is determined by different factors (light switch)

No exchange of information between lights	Lights can exchange phase information and form conjugation (optical phase conjugation)

When light enters one media, its direction of propagation changes because of the change in velocity, which is called refraction. However, for some anisotropy materials, another situation called birefringence, or birefraction, appears. In 1669, Rasmus observed the situation that in calcite, the crystal has more than one refractive lights and it could double the image below when rotated. In the 19^{th} century, this phenomenon is explained in terms of polarization. The arrangement of crystal structure determines that there is a single direction governing the material's optical anisotropy which is often known as the optical axis of the material so that all directions perpendicular to the axis are equivalent. Lights propagating parallel to the optical axis (with the polarization perpendicular to the optical axis) are governed by the refractive index n_o ('o' for ordinary). In opposite, lights with the polarization in the direction of the optical axis enjoy the refractive n_e ('e' for extraordinary). One unpolarized light will be split into two when it enters the birefringent material not in the direction of optical axis. The ordinary ray sees the refractive index n_o and does not change its direction whereas the extraordinary bends and enjoys the refractive index between n_o and n_e. Birefringence is the basis of electro-optic (EO) effect, one important aspect of nonlinear optics.

In 1875, J. Kerr found that a box of isotropy liquid appeared the properties of uniaxial crystal when electrical field was applied. Liquid can be polarized by electrical field in just 10^{-9} second and the change in refractive index is proportional to the square of the strength of field.

This experiment starts the study of EO effect. In 1893, Pockels found that longitude electrical field could change the properties of some anisotropy crystals and produce extra birefringence which is linear to the strength of electrical field so the Pockel's effect is also called linear EO effect. In Pockel's cells, two crystals are aligned in opposite orientation which form the same optical axis. As a result, the material will contain many optically active molecular units. These units have extended electron conjugation which can be easily polarized by electrical field. The polarization, which determines properties like refractive index, respond linear to the electrical field. It has been confirmed that linear EO effect only exists in crystals lacking inversion symmetry.

Researchers have found several optoelectronic properties influenced by electrical field, mainly for the absorption of light and the refractive index. Information transportation and conversion between different carrier is common and the most popular method is information conversion between electron (digital devices like computer) and photon or optical signal (like the Internet). As the need for larger bandwidth has become evident from the 1980s, EO technologies woth fast response has been focused more often and more inorganic crystals with EO properties like lithium niobate ($NiNbO_3$), one kind of perovskite which has been studied a lot for EO effect. As is just said, EO effect of oxide perovskite has been investigated and reported, as well as the advantages in photovoltaic applications and solar cells of organometal halide perovskites $MAPbX_3$, so there is a question: What about the EO properties of organic halide perovskites? Compared to inorganic perovskite crystals, the convenience of organometal halide perovskites in its possibility for soluble processing, making it more valuable for study[33].

Fabry-Perot Interferometer

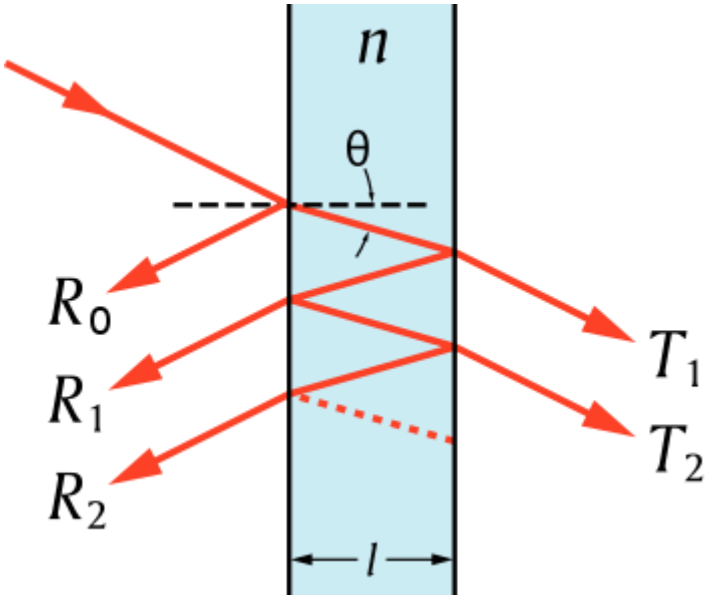

Figure 3 Structure of Fabry-Perot interferometer

In order to calculate the EO constant and judge the crystal of $MAPbX_3$ in the samples, the halide perovskite is made as a film between two metal layers so the EO effect can be measured in a Fabry-Perot interometer (FPI) or etalon. A FPI is made of two highly reflective mirrors. When the frequency of incident light, the incident angle and the refractive index of the material between two mirrors satisfy some conditions, there will be peaks in the spectrum of the transmission light, so the parameters can be calculated from the spectrum of transmission light of FPI if other parameters are already known or can be measured by other methods. In an etalon, the optical path difference (OPD) is determined by the equation $\Delta L = 2nl\cos\theta$ where l is the thickness of the material. When the phase motion is not considered, the phase difference is given by the equation:

$$\delta = \left(\frac{2\pi}{\lambda}\right)\Delta L = \left(\frac{2\pi}{\lambda}\right)2nl\cos\theta$$

If the reflectivity of inner interfaces R is given, the function of the transmission T_e of the etalon is:

$$T_e = \frac{(1-R)^2}{1+R^2-2Rcos\delta} = \frac{1}{1+Fsin^2(\frac{\delta}{2})}$$

where

$$\mathrm{F} = \frac{4R}{(1-R)^2}$$

When the phase difference between two adjacent lights equals multiples of the wavelength, transmission T_e would approach it maximum and form a peak in the spectrum.

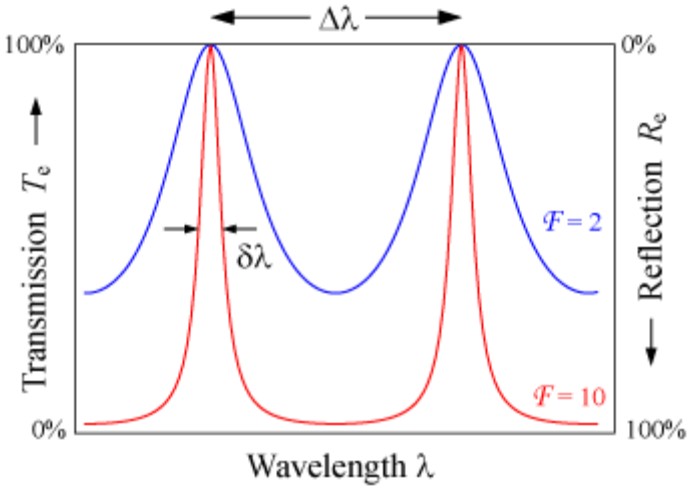

Figure 4 Relationship between transmission and wavelength in Fabry-Perot Interferometer

According to the function of transmission, the interval between two peaks is called free spectrum range (FSR). It is determined by the equation:

$$\Delta\lambda = \frac{\lambda_0^2}{2nlcos\theta+\lambda_0} \approx \frac{\lambda_0^2}{2nlcos\theta}$$

where λ_0 is the center of wavelength of the closest peak in the spectrum. The finesse of the spectrum is given by the ratio of FSR and half-width (the width of the peak in half the max height), which can be calculated by reflectivity when it is high enough (above 0.5). The function of transmission has four variables: refractive index, wavelength, thickness and incident angle, or sometimes called position. When the wavelength of the applied laser is ensured, the relationship between transmission light and position can be used to calculate the actual refractive index and thickness.

Chapter 2: Fabrication of metal mirrors

In a Fabry-Perot Interferometer, there are two metal layers above and below the material which works as two mirrors to reflect the incident light between them, in other words inside the perovskite film, and two poles to apply electric field on the sample. So there are some requirements for the properties of the pole, including the reflectivity and the surface morphology, which is influenced by the thickness of the layer. In this chapter, we will discuss crucial factors in the process of fabrication and the qualitative relationship between thickness and other properties.

Theoretical Model

From previous study, several groups have investigated the reflectivity of the silver (Ag) film of different thickness. J. Domaradzki reported a figure of the reflectivity of Ag in summary in 2016 34. In this figure, it is easily to find that the reflectivity of Ag thin film increases rapidly from small thickness but it will approach its maximum at one specific thickness and keep almost the same no matter how larger the thickness would be.

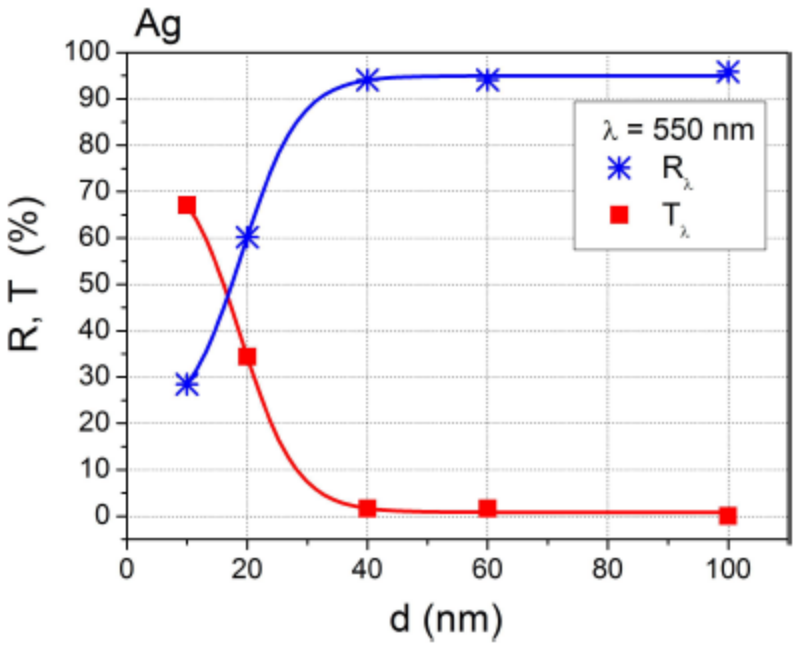

Figure 5 Relationship between transmission/reflection and thickness

However, there are several different mathematical models which can describe the tendency of the data from the figure. After plenty of studies, researchers mainly propose that the relationship between reflectivity and thickness could be in the form of logarithmic relation, so in this chapter, the data would be fit in this model and the error and variance are also analyzed.

Experiment

Ag film is deposited onto the surface of the glass slide by thermal evaporation in Edwards 306 Vacuum Coater. With the pressure at around $6*10^{-6}$ mbar, current is applied to the boat and silver is evaporated which will finally deposited as a layer of thin film on the glass slide. After fabrication, the thickness of Ag film is characterized with KLA Tencor Profilometer by measuring the thickness of the stage left on one side of the film. Then, the reflection ratio would be measured by Lambda 950 Reflector in the laser with the wavelength range between 1100 nm

and 1800 nm so that the reflection ratio in 1550 nm can be achieved from the average of a small rang with less error.

Discussion of data

Figure 6 Alignment of slides in thermal evaporator

As is shown in the figure above, slides are placed on the board of evaporator side-by-side so we can get three pieces once. In order to reduce the random error, each slide will be picked with three points in the left side, right side and the center to measure the thickness of the film, so for all three experiments, the average thickness and the variance of them will be calculated to see the details in the technology.

Table 3 Thickness of thermal evaporation

Sample		Thickness (nm)				Standard Deviation
		1	2	3	Average	
Time 1	1	46.3	49.5	46.9	47.6	1.39
	2	49.3	49.3	50.5	49.7	0.57

	3	41.5	44.4	45.3	43.7	1.62
	1	27	27	25	26.3	0.94
Time 2	2	27	29	27	27.7	0.94
	3	24	23	20	22.3	1.7
	1	24	24	26	24.7	0.94
Time 3	2	24	26	25	25	0.82
	3	22	21	19	20.7	1.25

Several messages can be collected from the data of all three experiments. The first one is that the way of align the glass slides on the board influences the distribution of thickness on them. As a result, samples on the sides tend to have thinner film than other samples in the center within the same conditions and the thickness on the same sample usually follows this law. At the same time, the value of the variance in thickness indicates that no matter how thick and where the sample would be, the absolute value of the variance does not change a lot. In other words, the smoothness does not increase or reduce with the change in thickness and the position of the samples.

After confirming the requirements for the aim thickness, the next step is to search for the relationship between the reflectivity R and thickness T. As is said above, researchers have considered it to be the logarithmic relation, so the equation could be:

$$\log T = kT + b$$

When it comes to the actual data, the logarithm of reflectivity should be linear to the change in the value of thickness.

Table 4 Reflectivity of silver film

Sample		Thickness (nm)	Reflectivity (%)
	1	47.6	99.79
Time 1	2	49.7	99.86
	3	43.7	99.39
	1	26.3	97.98
Time 2	2	27.7	98.16
	3	22.3	95.80
	1	25	97.06
Time 3	2	24.7	97.33
	3	20.7	91.84

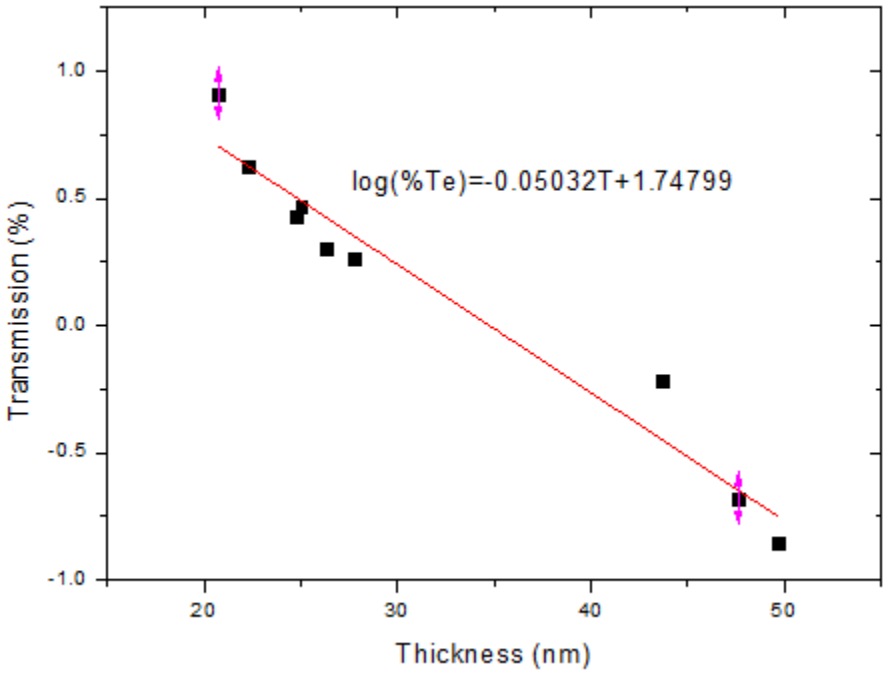

Figure 7 Relation between transmission and thickness

Although the logarithmic relationship has been proved by a number of studies, error still exists in the data and its value is different for each group of data. As a result, the degree of this linear correlation is different for every group. The linear relation between logarithm of the transmission ratio in per cent and thickness is strongest among all groups, so this group is used to find the fitting equation. The fitting equation of the transmission ratio and thickness shown in the figure is that:

$$\log \%Te = -0.05032T + 1.74799$$

The target value of the reflectivity of the metal mirror touched with incident light firstly is 95% and that of the other one is 99%. The result is that the 99% reflectivity is caused by one layer with the thickness of 34.73 nm and 95% reflectivity coms from 20.84 nm thickness.

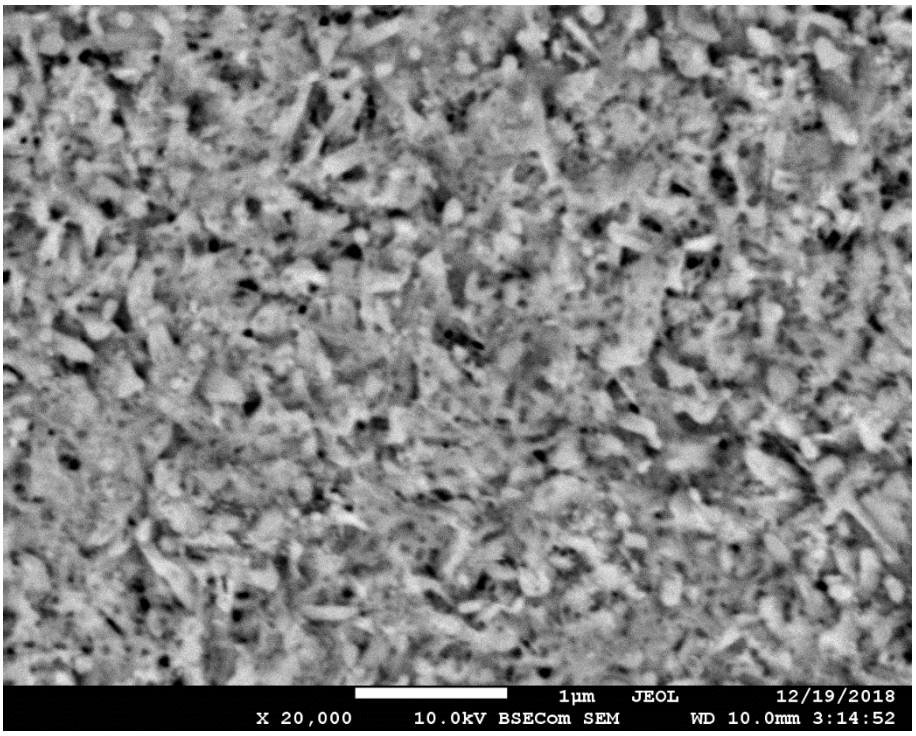
1µm JEOL 12/19/2018
X 20,000 10.0kV BSECom SEM WD 10.0mm 3:14:52

(a)

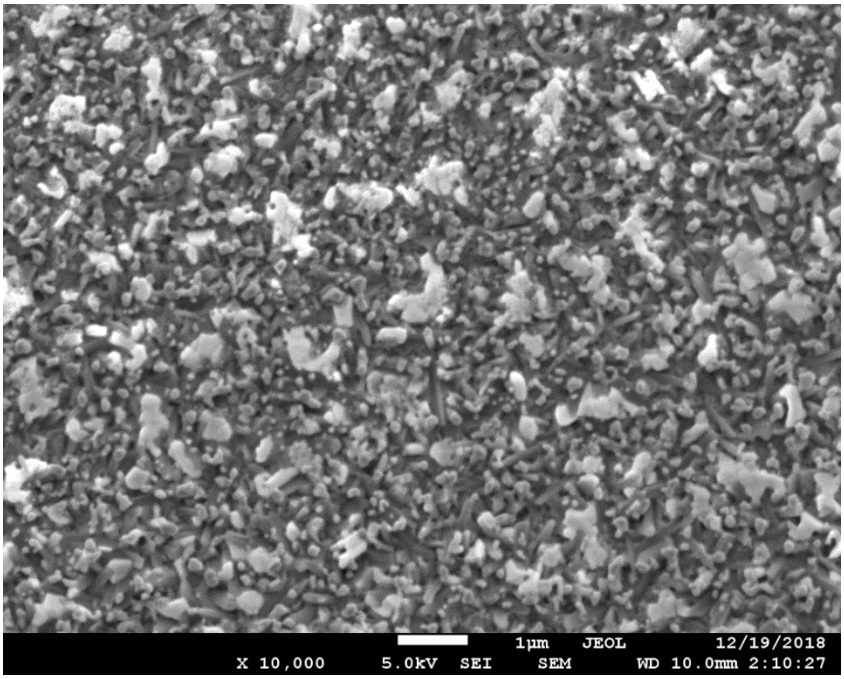
1µm JEOL 12/19/2018
X 10,000 5.0kV SEI SEM WD 10.0mm 2:10:27

(b)

Figure 8 SEM image for the silver film on the perovskite film (a) 20,000 times; (b) 10,000 times

However, in actual practice, it is unexpected that silver cannot form a smooth mirror on the surface of the perovskite film because of several unknown and strange reactions. From the SEM images of the failed silver pole, it is strange that many ‘mountains’ and ‘valleys’ appear which makes the film lacking its original high reflectivity. There are even many holes in the metal mirror which is cannot be accepted for following research. So gold is used to replace silver for depositing the metal mirror in that its capacity in this situation and the similar ability for reflecting far-infrared laser as silver has been proved in previous study. The problem is that the surface morphology of gold film is poorer than silver so there is little error in the transmission ratio in actual operation. This is one problem which can be optimized in further study.

Chapter 3: Factors for thickness and surface morphology of halide perovskite film

Possibility and advantage of fabrication in soluble process

One great advantage of organometal halide perovskite $MAPbX_3$ is the possibility in solution process. For other EO materials like lithium niobate $NiNbO_3$, one kind of oxide perovskite mentioned above, the method of crystal growth is difficult, usually depending on complex process with expensive facilities like physical vapor deposit (PVD), chemical vapor deposit (CVD), ion implantation, molecular bean epitaxy (MBE) and so on. Solution based crystal growth method has been investigated and reported by scientists all over the world for organic halide perovskites and similar material like $CsPbX_3$[35-41], although they are also often accompanied by extra technologies like high applied pressure[36], high vacuum[39] and gas treatment[38,39]. In this project, spin-coating method is used for the preparation of organic halide perovskite $MAPbI_3$ film for the convenience in practice.

In spin-coating process, factors for the thickness including the velocity, the concentration of the solution with suitable solvent and the flow of gas if gas treatment is necessary. The final properties representing the quality of the film are the thickness and morphology. Requirements for the thickness is from the next step where larger thickness can lead to better results of transmission ratio in the Fabry-Perot interferometer which makes itself easier for equation fitting with less extra treatment whereas requirements for better surface morphology are directly related to clear shape of the curve in the transmission figure. In 2015, researchers successfully realized solar cell made of halide perovskites with great breakthrough in efficiency33. Their article is worth considering and referring since the common recipe for preparing the solution and the simple conditions of soluble process.

It is mentioned in Chapter 1 that linear EO effect only exists in crystals lacking inversion symmetry. In other words, the perovskite film must be polarized or at least has polarity. This recipe chooses heating and annealing to finish this process. This is why heating and annealing are important in this process and more details will be discussed in the following chapter.

As the most important factors are the spinning velocity and solution concentration and the properties showing the quality are thickness and surface morphology, different conditions will be tried in order. Experiments start with the low concentration used in the related article33 to figure out the influence of spinning velocity, finally obtaining the coefficient and calculating the specific function. The influence of different factors in spin-coating process has been analyzed and the relation of thickness and spinning velocity is reported by N. Sahu and his co-worker42. In their article the velocity in the direction of each radius ix considered to transfer the relation of thickness and time to that and position. After evaporation rate is included, the accurate expression of thickness is given from integral calculation. Ignoring the change in the humidity of air and the flow, the thickness h is defined as:

$$\mathrm{h} = \left[\frac{3C^2(t)\vartheta_0\varphi}{2\{1 - C_0(t)\}\omega^2}\right]^3$$

When only the rotation rate is considered and other variables can be ignored as constants, the relation can be given as $\mathrm{h} \propto \omega^{-2/3}$.

Experiment

To get the solution of $MAPbI_3$, pure solid MAI and PbI_2 are prepared as the raw material. Anhydrous N,N-dimethyformamide (DMF) and dimethyl sulfoxide (DMSO) are chosen as the solvent for the high solubility of our raw material. The mixing solvent used in practice for

dissolving MAI and PbI_2 is composed of DMF and DMSO in the ratio of 9:1 in volume in order to keep the high solubility and reduce the usage of diethyl ether for washing out the residual DMSO. MAI and PbI_2 are dissolved in the mixing solvent both in the concentration of 1.4M (0.227g/ml for MAI and 0.658g/ml for PbI_2) and shaken on the machine Vortex 2 to get transparent solution with filtration by Syringe Filter. At the same time, glass slides are cut into pieces in the size of 1 inch*1 inch. Before spin-coating, the glass slides are cleaned by acetone and isopropanol (IPA) in ultrasonic for 15 minutes each and processed by O_2 plasma for 10 minutes after being dried by nitrogen gas. The $MAPbI_3$ solution is dropped on the center of pieces of cleaned glass and the rotating process continues for 25 seconds with diethyl ether washing in the last 10 seconds. Finally, the samples are annealed in 100℃ for 10 minutes. At this time, the thickness is still measured by KLA Tencor Profilometer.

Discussion

Thickness

Table 5 Thickness of perovskite film in different rate

Speed (rpm)	Thickness (nm)		Average	Modified Value
	1	2		
4000	245	245	245	0.003969
3000	431	431	431	0.004807
2000	616	641	628.5	0.0063
1000	758	812	785	0.01

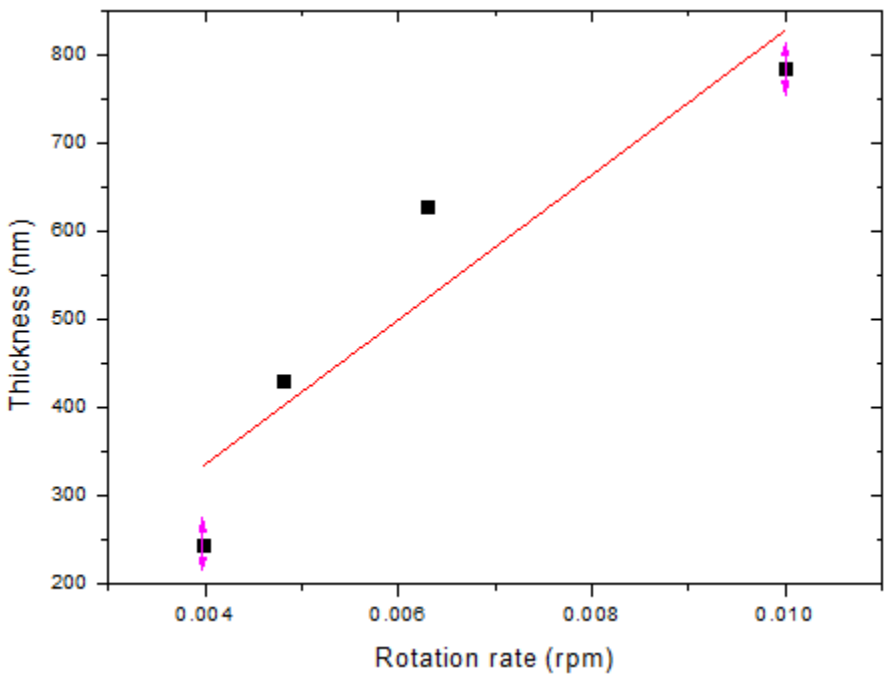

Figure 9 Fitting line of thickness over rotation rate

In order to get peaks in the transmission figure, the ideal thickness is more than half the wavelength of the 1550 nm laser so it needs to be more than 725 nm. However, from simulation of the transmission, peaks can be found both at 600 nm and 350 nm. The relation of rotation rate and thickness is given from the fitting line in the figure:

$$\mathrm{T} = 8.219 \times 10^{4} r^{-2/3} + 7.1173$$

To get perovskite film with the thickness of 725 nm, the rotation rate should be 1225 rpm. Considering the practice in actual experiments, samples made in 1500 and 2000 rpm have been used for testing the surface morphology. However, there can be seen great error for the fitting line and the data. The trend for data is more similar to quadratic polynomial or logarithm, so these models have also been tried for the experimental data. Opposite to what is assumed from the figure, error in these models in much larger than that of the original model from previous

research. In conclusion, error comes from factors other than mistake in the model like the error in real velocity and the smoothness of the film, or even in profilometer so it is hard to reduce this error by taking more experiments. The solution to this problem is to fit the data in the following experiment to achieve the real thickness and the corresponding shape. As a result, the surface morphology has become the most important factor for evaluation of the film. However, the influence of concentration has not been investigated in this project. Further studies in related directions can pay more attention to the influence of the change in the ratio of the mixing solvent and the concentration of the solution.

Morphology

(a)

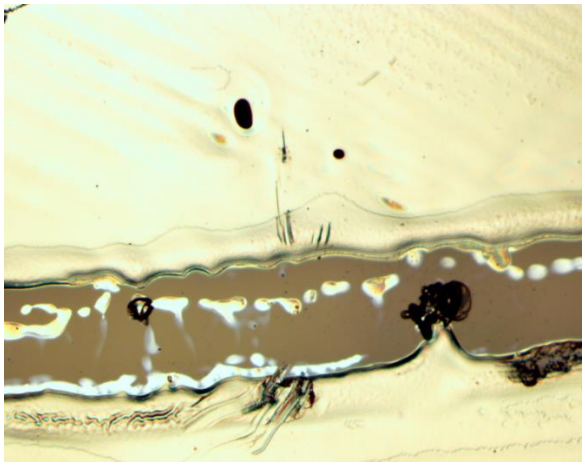

(b)

(c)

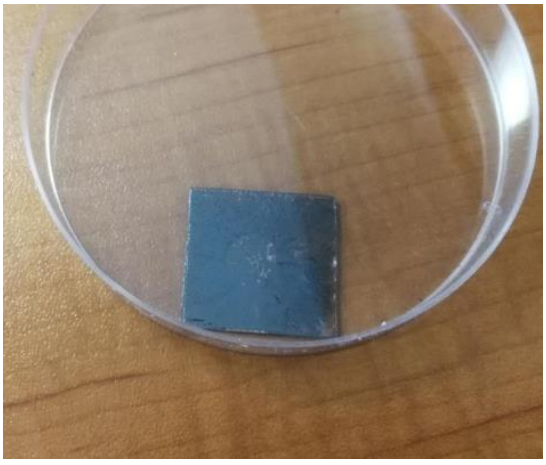

(d)

Figure 10 Surface morphology of different film (a) surface of 1500 rpm sample; (b) cracks in microscopic; (c) surface of 2000 rpm sample; (d) surface of 1000 rpm failed sample

Above are pictures of the surface of the chosen samples. It is clear that the quality of surface decreases with the reduction in rotation rate, even causes failed sample when it is low enough. Cracks with bare glass distributed across the surface, which is not tolerable for the following examination. However, what is the quality of those samples with highly reflective and smooth surface in molecular scale? Would there be some leakage not visible by eyes?

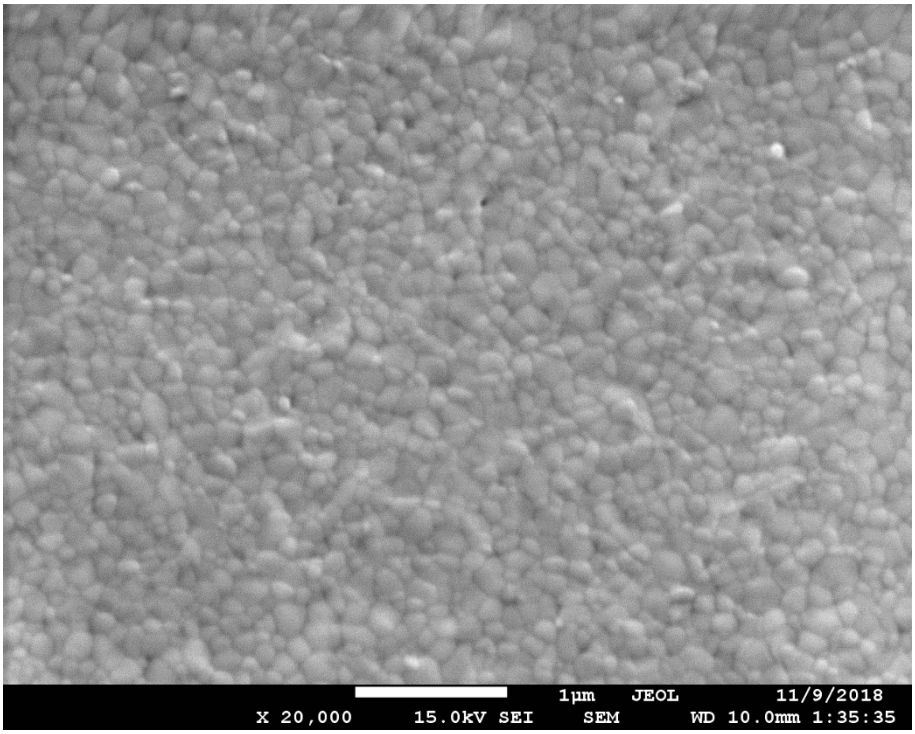

(a)

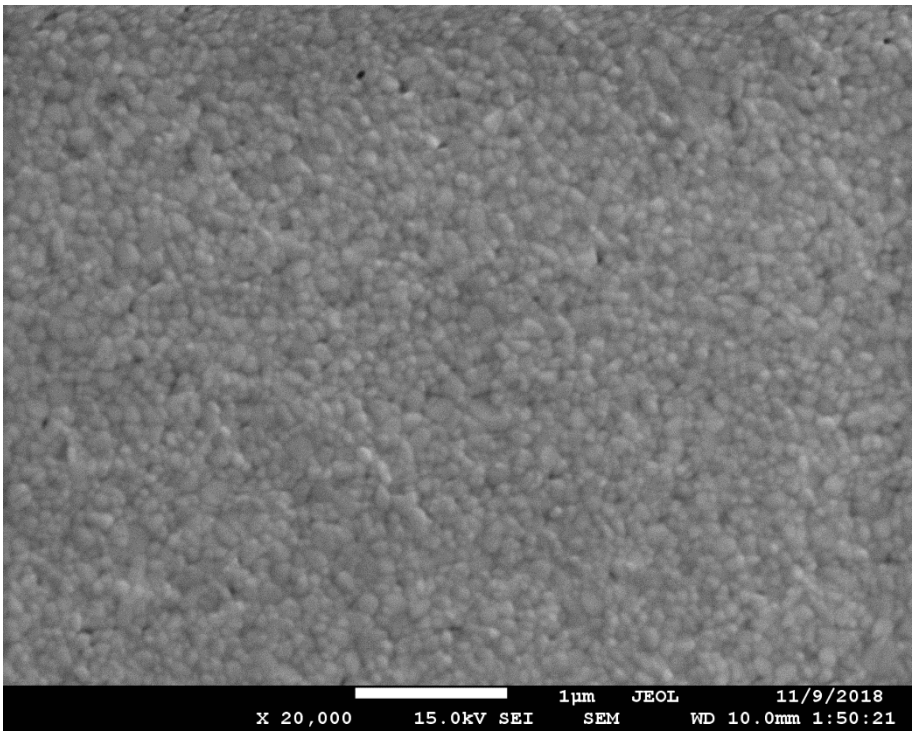

(b)

Figure 11 SEM images of perovskite film (a) sample of 1500 rpm; (b) sample of 2000 rpm

Detailed information of the surface morphology is given from the SEM images. Both samples do not contain isolated particles on the surface which means that each film is continuous in its highly reflective area. However, irregularity can be noticed in 20,000 times and the radius of the particles on the surface of film from low rotation rate is larger than that on the surface of samples from higher rate. The conclusion is that decrease in rotation rate can result in higher irregularity of the surface even if these films are thicker.

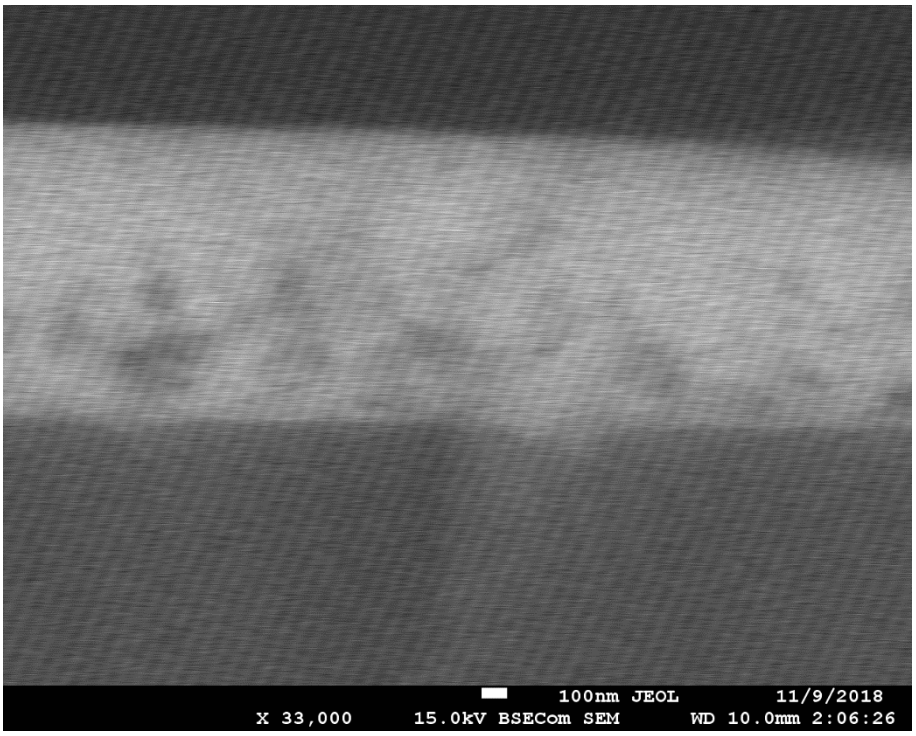

(a)

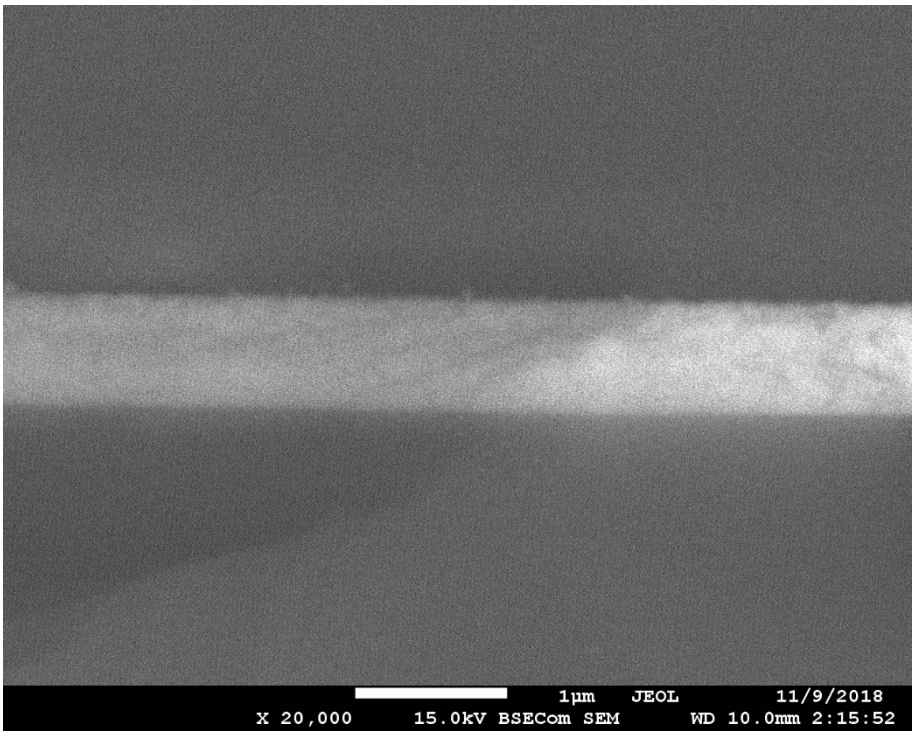

(b)

Figure 12 Cross-section SEM images of film (a) sample of 1500 rpm; (b) sample of 2000 rpm

The images of cross-sectional area indicate the uniformity of the film. It is easy to find that the film prepared in low rotation rate is less even in its thickness. The variance of thickness would be much larger so the real thickness is hard to control. For all these reasons, 2000 rpm is the most suitable rotation rate for the recipe by present. Again, the influence of different concentration has not been finished so it is only the best choice of present researchand recipe.

Chapter 4: Characterization of EO coefficients and analysis of related effects

After successful fabrication of the Fabry-Perot cavity of organic halide perovskite film, the characterization of the EO coefficients can be realized by the examination of the transmission ratio and the changes in refractive index caused by electric field. However, no one can confirm the EO effect just by the linear response of electric field, so extra test is necessary for other effects with their specific changes.

Theory for the Fabry-Perot Method

With the request of finding a simple method to quickly screen EO material, in 1990 Teng and Man as well as Schildkraut both proposed the measurement of EO coefficients using a reflective arrangement seperately43,44. In 2006, Park reported his analysis of Teng-Man technology considering multiple reflection between metal layers45, and the application of this theory into practical experiments in following research in 2011 using Fabry-Perot method46.

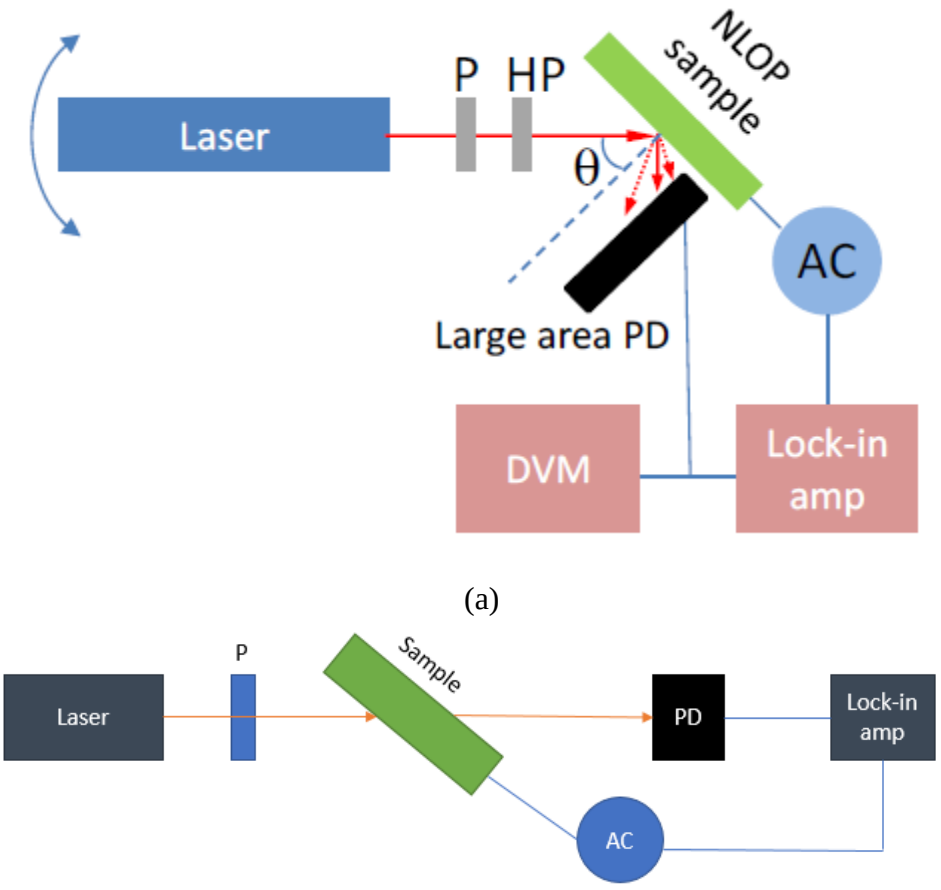

Figure 13 Facility for Fabry-Perot Interferometer (P-polarizer, HP-half wave plate, PD-photodetector, DVM-digital voltmeter) (a) Facility to measure reflection; (b) Facility to measure transmission

In their facility, the reflective signal of the polarized light is collected by large area photodetector near the sample and data is passed to lock-in amplifier in the signal-position scanning to make sure of the angle of the smallest reflection. Then electric field is applied to the sample in the found angle and the difference in response is also collected by lock-in amplifier and used for calculation of EO coefficient. In this experiment,

The mathematical model starts from the term of the phase of the polarized light:

$$\Psi^{(\gamma)} = k_0 n_\gamma cos\theta_\gamma d$$

where $k_0 = \lambda/2\pi$ is the wave vector. λ is the wavelength of polarized light. n_γ is the refractive index of different modes and γ represents the mode of polarization, s- for TE mode and p- for TM mode. θ_γ is the reflective angle for each mode and d is the thickness. Only when $\Psi^{(\gamma)} = m\pi, m = 1,2,3 \ldots \ldots$ can the reflection reaches its minimum. Since the internal angle can be calculated from the incident angle and the refractive index, this term could be represented in the external incident angle θ and can be written as:

$$\Psi^{(\gamma)} = k_0 d\sqrt{n_\gamma^2 - sin^2\theta}$$

by Snell's law. When an external electric field is applied to the sample, both the refractive indices for ordinary and extraordinary light n_o and n_e will change and it is related to the incident angle and the original refractive index. As is just mentioned, $\Psi^{(\gamma)} = m\pi, m = 1,2,3 \ldots \ldots$ at the minimum reflection, the term for the change can be represented by the derivative of refractive index n_γ with respect to the exterior incident angle θ by setting the total differential of phase equal to 0 ($d\Psi^{(\gamma)} = 0$):

$$\frac{\partial n_\gamma}{\partial \theta} = \frac{sin2\theta}{n_\gamma} \approx \frac{\Delta n_\gamma}{\Delta \theta}$$

The true meaning of the term above is that the change in refractive index can be finally calculated from the angular shift $\Delta\theta$. However, there are two problems in actual experiment: the first is there is no direct method for the measurement of the angular shift; then the angular shift is determined by both the slope of reflection $dR/d\theta$ and the value of optical density. These problems cause the final choice in the experiment.

First of all, the modulated refractive indices Δn_o and Δn_e can be achieved from the term by the angular shift $\Delta\theta$. It is obvious that $\Delta n_o = \Delta n_s$ directly. Δn_e can be obtained from Δn_s and Δn_p and the corresponding index ellipsoid for a uniaxial anisotropy crystal[47]:

$$\frac{1}{n_p(\theta_p)^2} = \frac{cos^2\theta_p}{n_o^2} + \frac{sin^2\theta_p}{n_e^2}$$

$$n_p(\theta_p)^2 = n_o^2\left(1 - \frac{sin^2\theta}{n_e^2}\right) + sin^2\theta$$

By differentiation, the new term is:

$$\Delta n_p = \frac{1}{n_p}\left[n_o\left(1 - \frac{sin^2\theta}{n_e^2}\right)\Delta n_o + \frac{(n_o sin\theta)^2}{n_e^3}\Delta n_e\right]$$

Finally, the solution for Δn_e comes from the term:

$$\Delta n_e = \frac{n_e^3}{(n_o sin\theta)^2}\left[n_p\Delta n_p + n_o\left(\frac{sin^2\theta}{n_e^2} - 1\right)\Delta n_o\right]$$

Because the crystal structure of the $MAPbI_3$ is considered to be belonging to the point group ∞mm (space group $C_{\infty v}$), the EO coefficient comes from:

$$\Delta n_o = -\frac{1}{2}n_o^3 r_{13}\frac{V}{d}$$

$$\Delta n_e = -\frac{1}{2}n_e^3 r_{33}\frac{V}{d}$$

and in the assumption, the value of r_{33} should be three times of that of r_{13}.

The system of characterization in this project is a little different of the system from previous study. In this research we choose the transmission instead of reflection because the more simple facility and the lower background so that the peak can be distinguished more easily. In order to solve the problem of the measurement of the weak signal of angular shift, the electric field is applied at the position in the incident angle where the transmission ratio is half the value of the peak. At this position, the relation of transmission and incident angle are closest to linear relation so the slope $dTe/d\theta$ reaches the maximum and the ratio of optical density over the noise is high enough to distinguish. So the linear relation can be applied to several points nearby and the angular shift $d\theta$ can be achieved from the change in transmission ratio with the term.

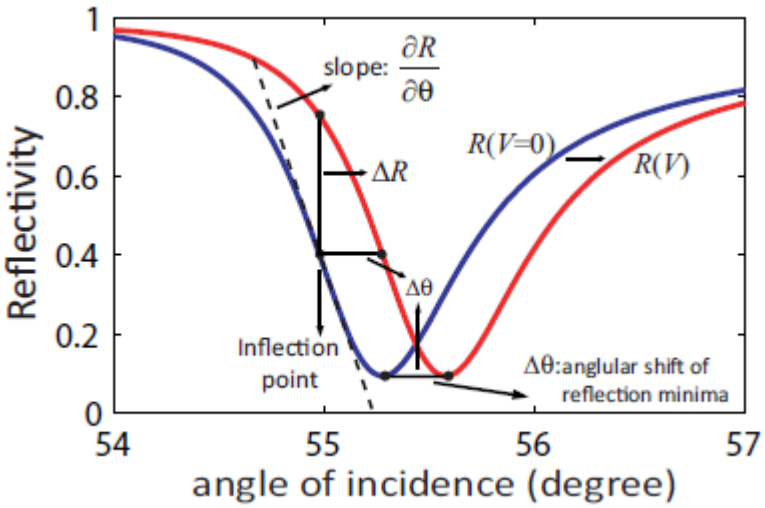

Figure 14 Specific relation in this experiment

One more difference is from the slope. In the previous research, the slope $dR/d\theta$ is negative. Ignoring scattering of the metal mirror and the surface of organic halide perovskite film, the relationship of reflectivity R and transmission Te is $R + Te = 1$, so the shape of the transmission curve is same as that of reflection curve with the opposite slope. As a result, the

slope of transmission $dTe/d\theta$ is positive and there is no minus before the term of the change in refractive index.

Experiment

The preparation in the previous two steps is repeated before characterization. Glass slides are cut into suitable sizes and cleaned with acetone and IPA in ultrasonic. These pieces of glass are then processed by the O_2 plasma from the Asher Plasma Etch. Polymer masks with specific shapes are put above these small slides to get the ideal silver bottom pole. Then before the spin-coating process, the slides with bottom silver metals are treated by acetone, IPA and even plasma again. The spin-coating process is conducted in several selected rotation rate around 2000 rpm. The following final step is the thermal evaporation of the top silver layer with special shape with partly superposition to form a Fabry-Perot etalon.

After the fabrication of the Fabry-Perot cavity, samples are firstly scanned for a large range of incident angles. A chopper with specific frequency is used to leave this frequency in signal so noise can be filtered. Conex-cc is used to drive the motion of the rotator while all information of it and the light signal collected by the SR830 lock-in amplifier can be stored and read from the data card KI-488. Then voltage is applied to the sample at the incident angle of half the peak. Signal of a sine wave and a square wave with the same frequency is in output. The former is applied to the sample and the latter is connected to the lock-in amplifier in 4V as a reference. The strength of the collected polarized light is displayed in the form of voltage so the change in transmission ratio can be obtained to calculate the angular shift.

Discussion

Content analysis

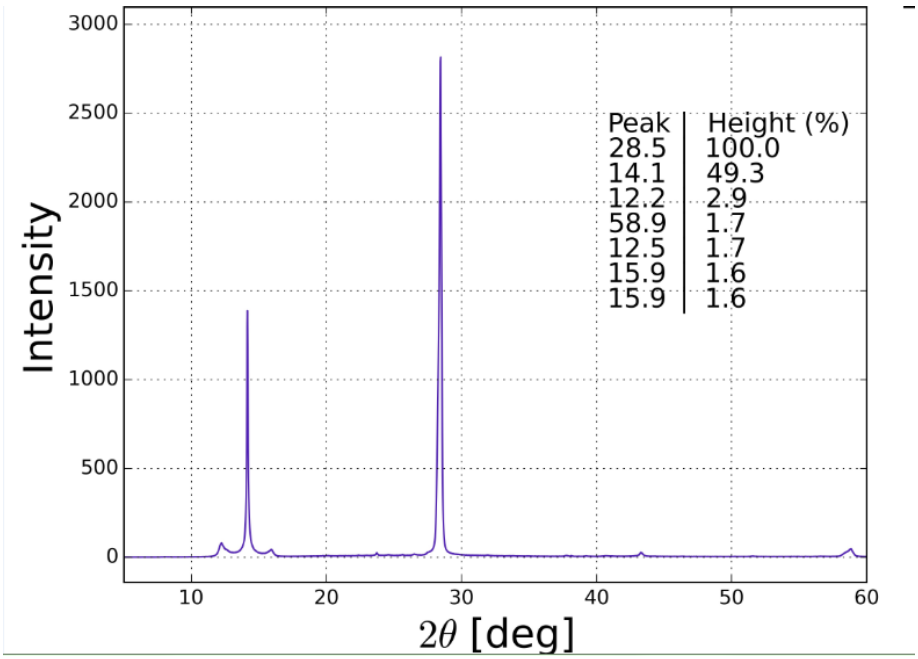

(a)

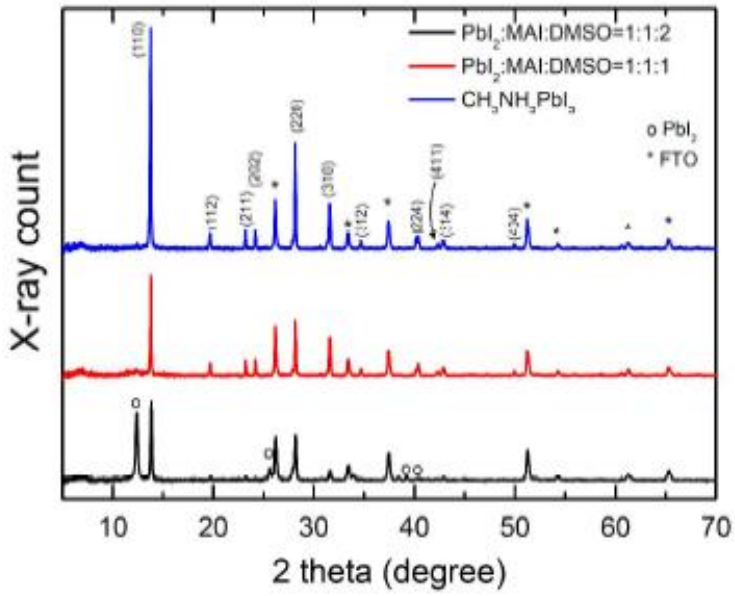

(b)

Figure 15 XRD pattern for MAPbI3 (a) sample (b) reference

There are two clear peaks in the XRD pattern of the scanned sample, one in 14.1 degree and another in 28.5 degree. Compared to the standard XRD pattern of $MaPbI_3$ in solar cell, it is easy to find the peak of (110) and (220) for $MAPbI_3$ crystal in this sample. However, without the crystal XRD scanning, the actual crystal structure of the organometal halide perovskites film in the sample cannot be confirmed, which needs to be find in experiment.

Data and fitting

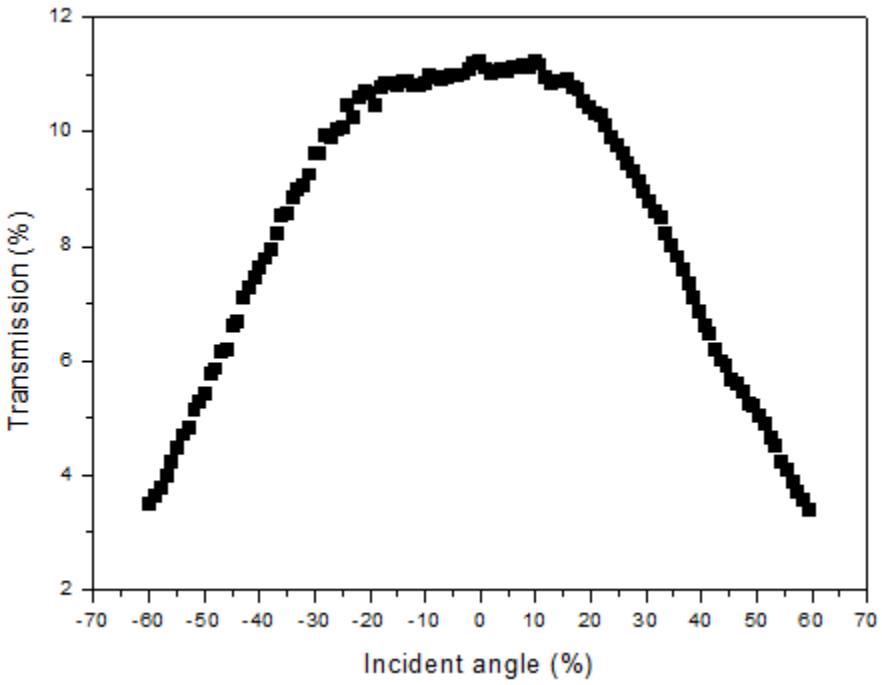

(a)

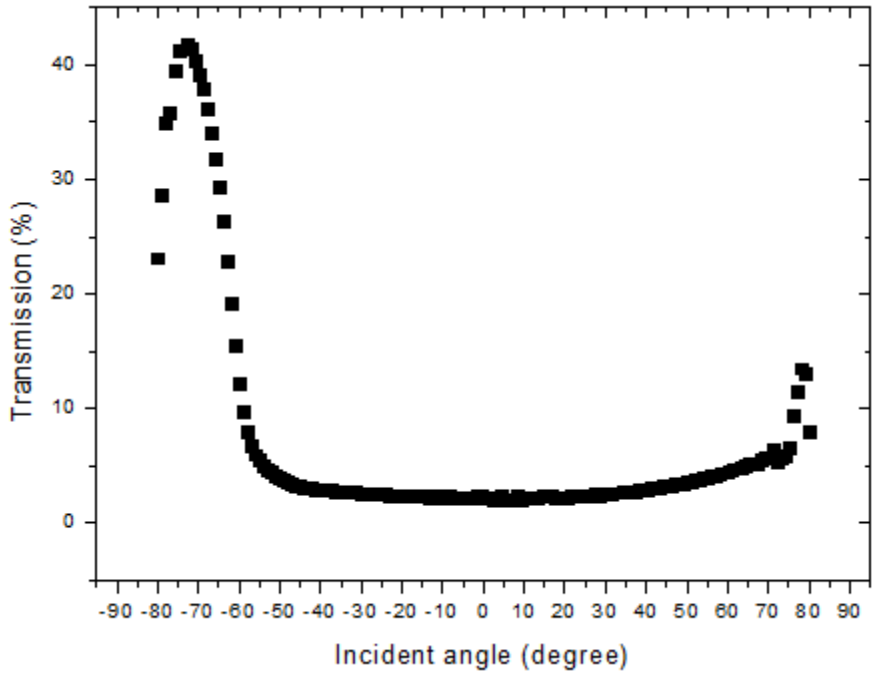
Transmission (%)
0
10
20
30
40
-90 -80 -70 -60 -50 -40 -30 -20 -10 0 10 20 30 40 50 60 70 80 90
Incident angle (degree)

(b)

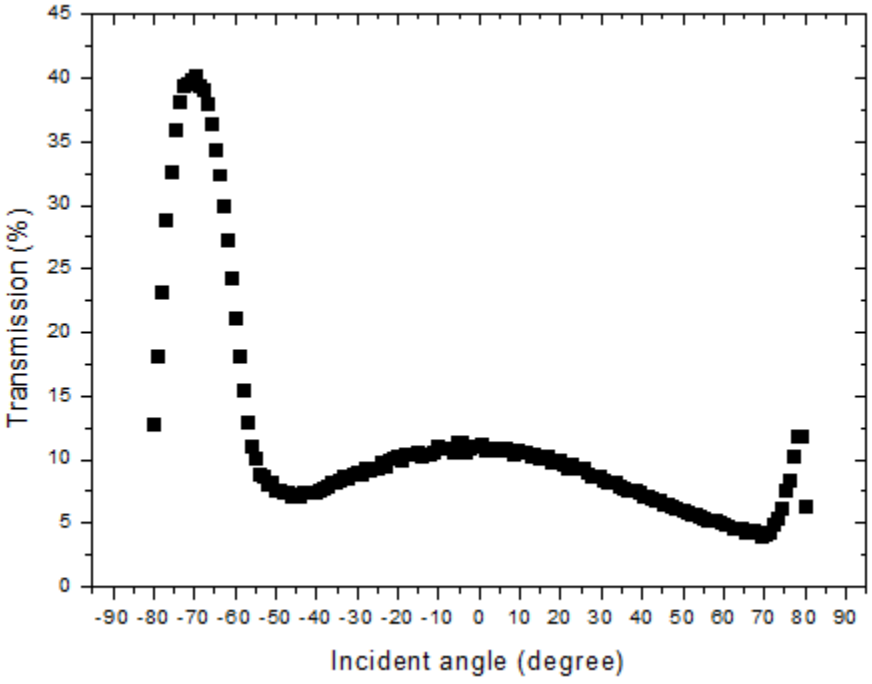
Transmission (%)
0
5
10
15
20
25
30
35
40
45
-90 -80 -70 -60 -50 -40 -30 -20 -10 0 10 20 30 40 50 60 70 80 90
Incident angle (degree)

(c)

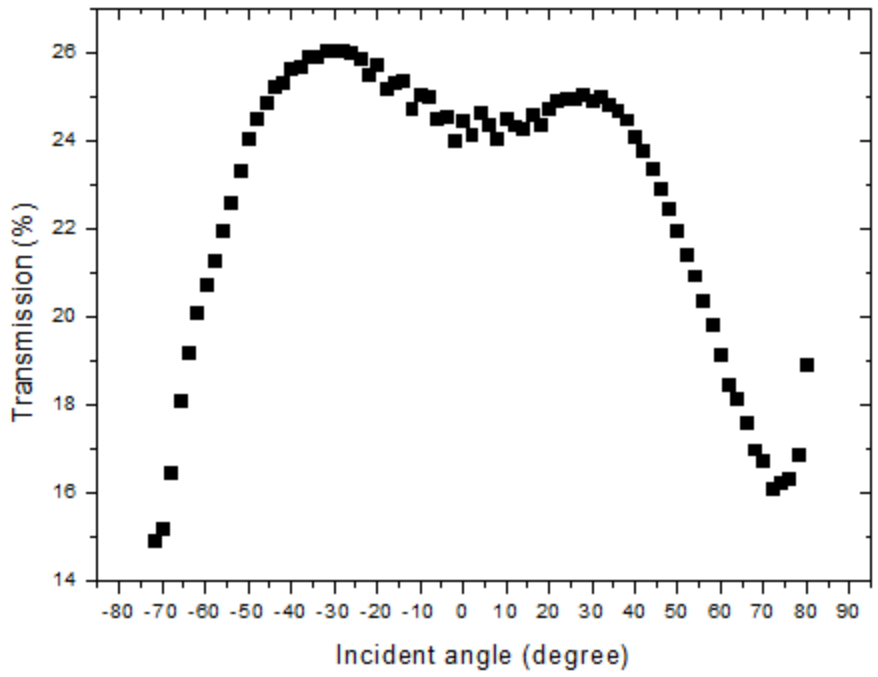
Transmission (%)
26
24
22
20
18
16
14
-80 -70 -60 -50 -40 -30 -20 -10 0 10 20 30 40 50 60 70 80 90
Incident angle (degree)

(d)

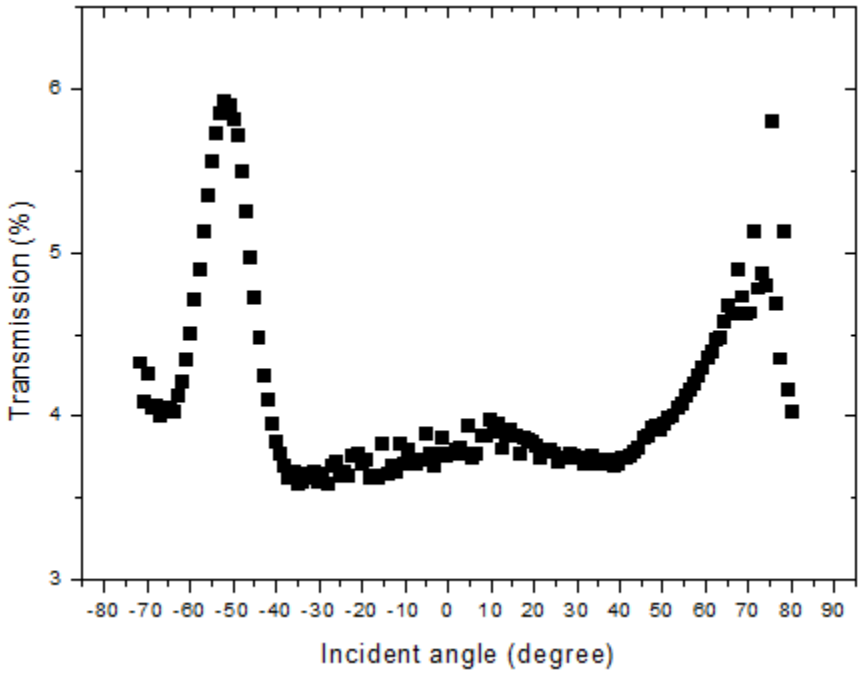
Transmission (%)
6
5
4
3
-80 -70 -60 -50 -40 -30 -20 -10 0 10 20 30 40 50 60 70 80 90
Incident angle (degree)

(e)

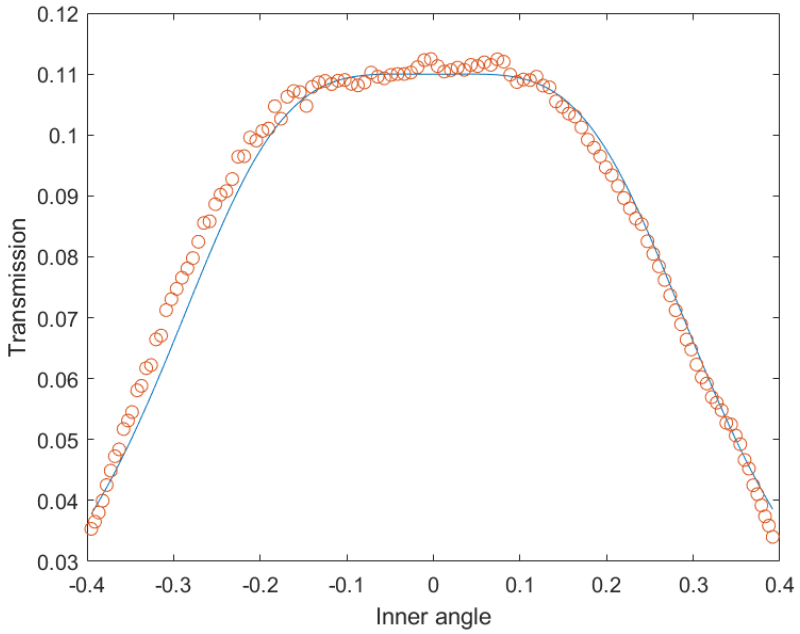
Transmission
Inner angle
0.12
0.11
0.1
0.09
0.08
0.07
0.06
0.05
0.04
0.03
-0.4
-0.3
-0.2
-0.1
0
0.1
0.2
0.3
0.4

(f)

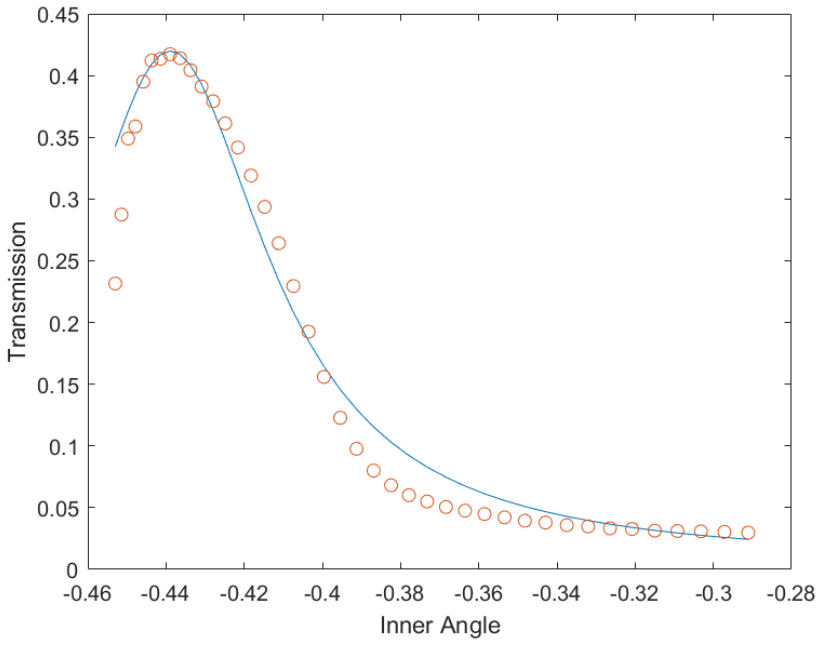
Transmission
Inner Angle
0.45
0.4
0.35
0.3
0.25
0.2
0.15
0.1
0.05
0
-0.46
-0.44
-0.42
-0.4
-0.38
-0.36
-0.34
-0.32
-0.3
-0.28

(g)

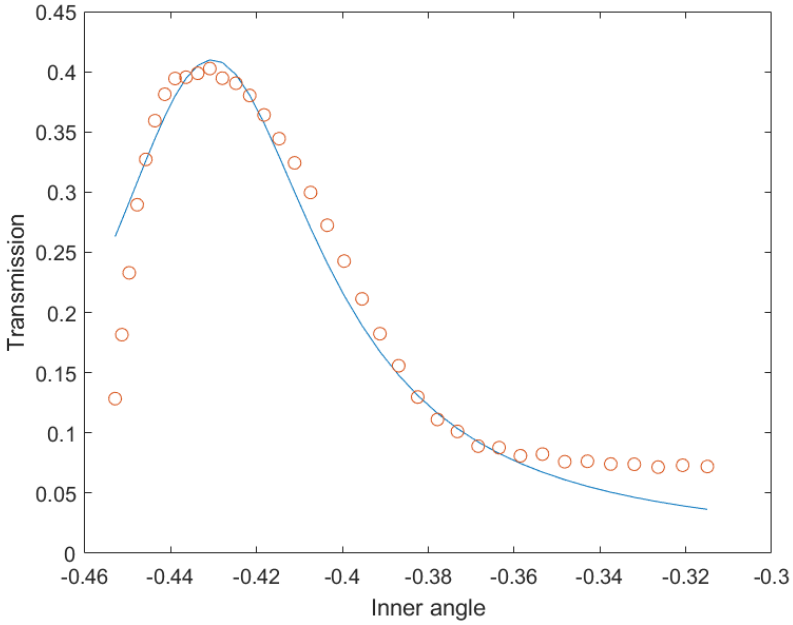
Transmission
Inner angle
0.45
0.4
0.35
0.3
0.25
0.2
0.15
0.1
0.05
0
-0.46
-0.44
-0.42
-0.4
-0.38
-0.36
-0.34
-0.32
-0.3

(h)

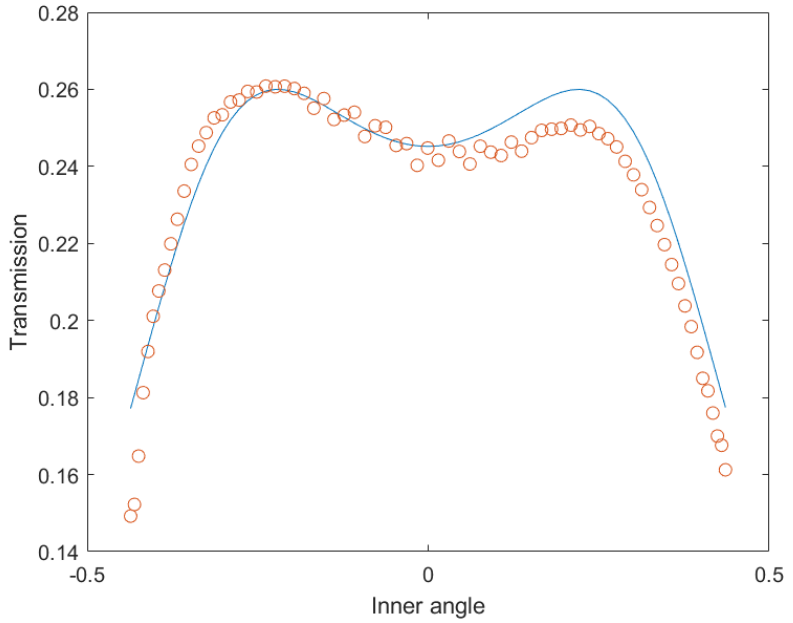
Transmission
Inner angle
0.28
0.26
0.24
0.22
0.2
0.18
0.16
0.14
-0.5
0
0.5

(i)

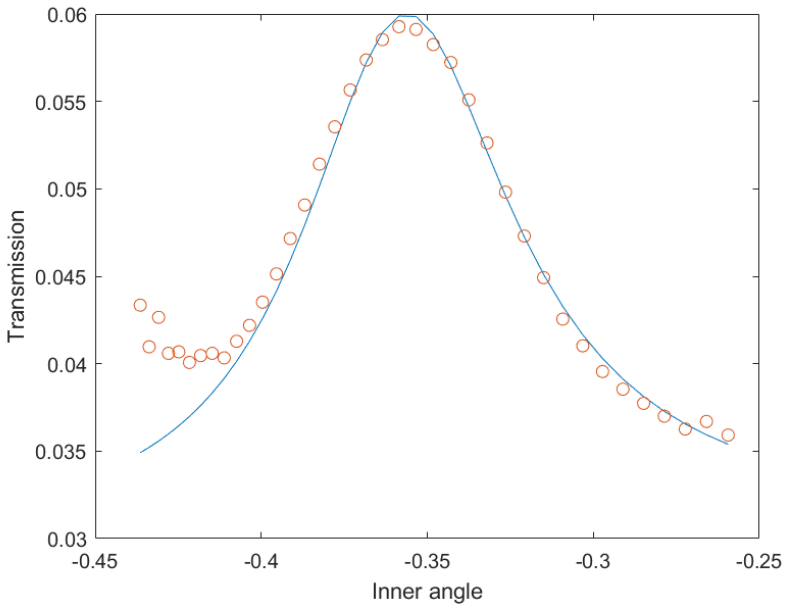

(j)

Figure 16 Figures of transmission vs. incident angle (a) sample 02 TE mode; (b) sample 02 TM mode; (c) sample 03 TE mode; (d) sample 03 TM mode; (e) sample 01 TE mode; (f) – (j) corresponding fitting curve

Above are the transmission-position figures of samples. All of them are fit by the term of transmission introduced in Chapter 1:

$$T_e = \frac{(1-R)^2}{1+R^2-2Rcos\delta} = \frac{1}{1+Fsin^2(\frac{\delta}{2})} = \frac{1}{1+Fsin^2(\frac{2\pi}{\lambda}nlcos\theta)}$$

Clear information from the term is that there should be two symmetric peaks in the figure and obvious error exists. In this project, system error mainly comes from the alignment of devices and the sample. The figures containing two whole peaks are used to confirm the system error.

Results from the data indicates that the shift in the coordinate of incident angle is quite tiny so the existing axis could be considered as the vertical axis of transmission. The height of both

peaks is also different possibly called the linear incline caused by the tilt in the alignment of sample on the rotator, which is proved by the incline in the baseline of other figures with only one peak in the left. After eliminating the linear incline, for both the refractive indices of the ordinary and extraordinary light of 2.25 (the difference between these two values are starting from thousands which is beyond the accuracy of measurement and calculation), the thickness can be achieved from the position of the peak.

Table 6 Calculated thickness

Sample	Thickness (nm)		Average
	TE	TM	
01	735.5	\	735.5
02	689.5	796.1	725.3
03	758.4	706.8	732.6

Calculation for r_{13}

Then alternating current voltage would be applied to the samples at the position of half-peak-height incident angle and the change in received optical density is read from the lock-in amplifier in the term of voltage. The reality is that the EO effect is a extremely weak signal so sometimes only the enlarged signal from the pre-amplifier can be detected by lock-in amplifier.

Table 7 Response for applied voltage

Response (μV)	Incident angle (degree)	Applied AC voltage (V)					
		3	6	9	12	15	18

01	TE	-55	4.6	8.6	13.9	17.6	21.3	26.6
	TM	/	/	/	/	/	/	/
02	TE	-62	/	0.38	0.57	0.89	0.93	1.28
(200*)	TM	-65	/	0.37	0.96	1.58	1.80	2.31
03	TE	-55	2.97	5.15	7024	8.63	10.88	13.37
(200*)	TM	-45	/	1.60	2.33	2.88	3.70	4.61

The calculation of r_{31} depends on the data in TE mode. The angular shift $\Delta\theta$ can be acquired from the response voltage at the position with most linear response.

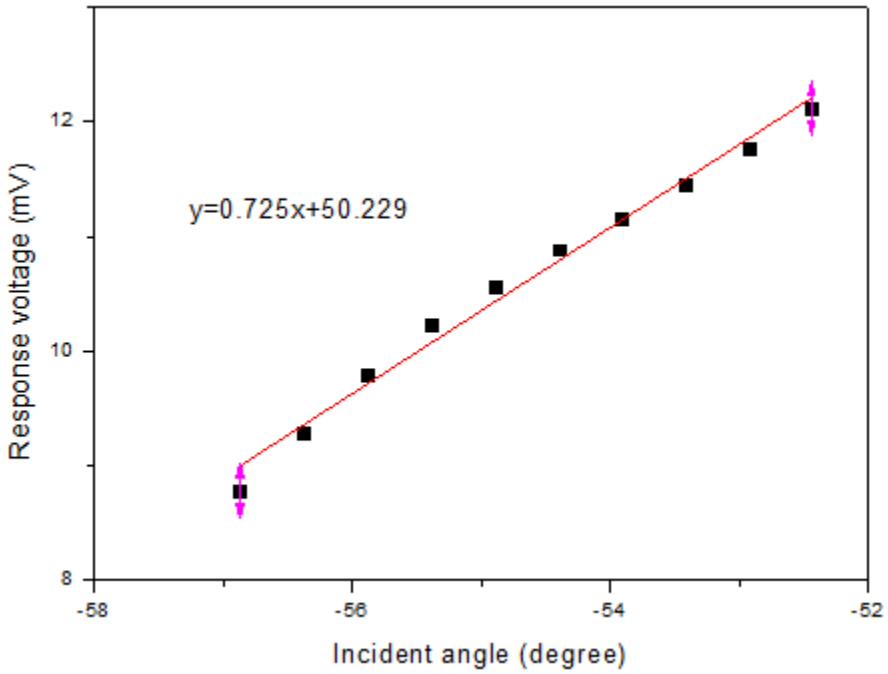

(a)

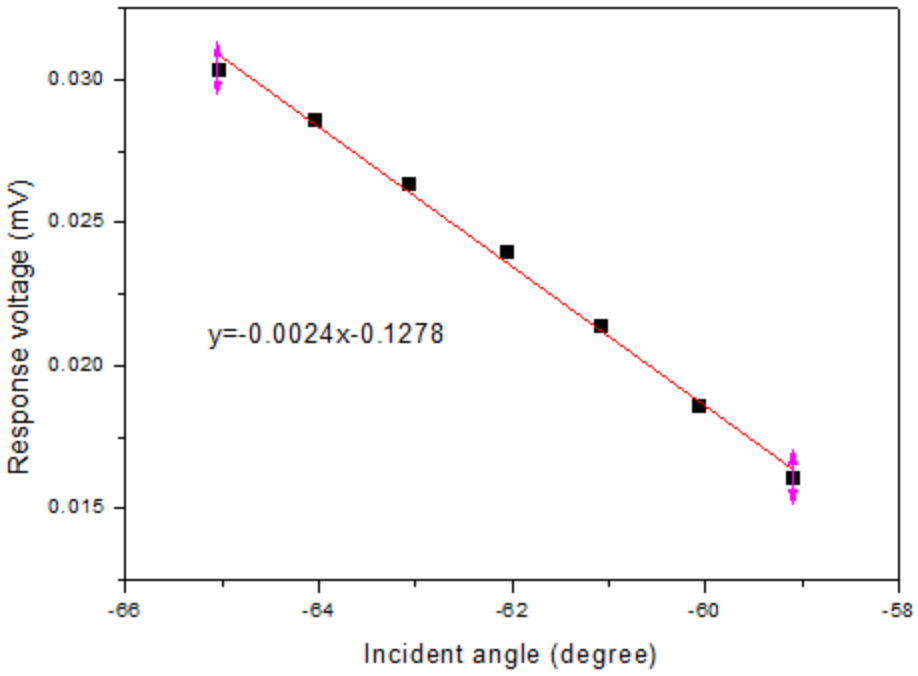

(b)

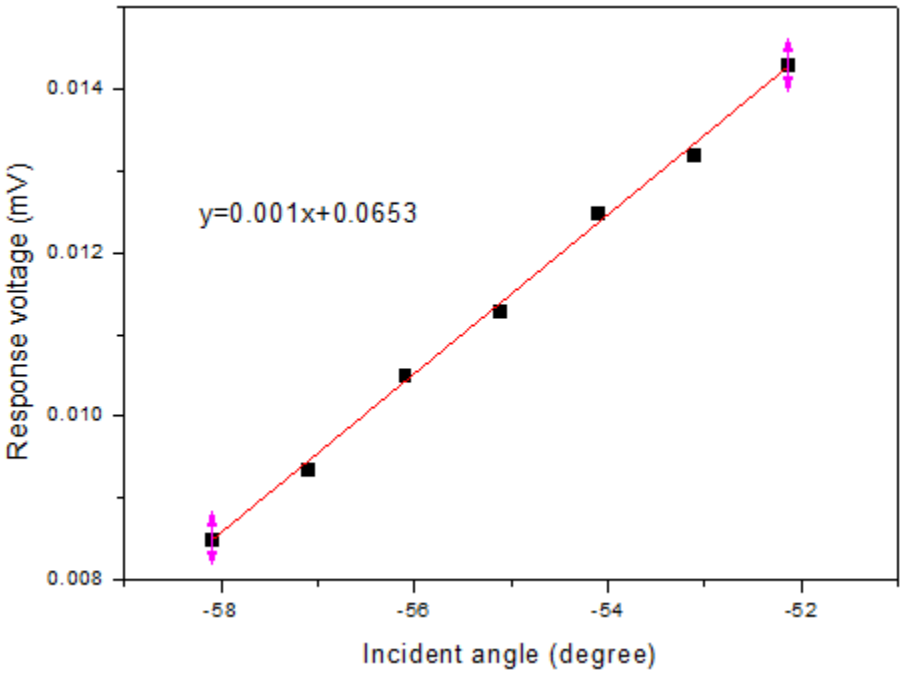

(c)

Figure 17 Linear fitting of TE transmission at half-peak-height (a) sample 01; (b) sample 02; (c) sample 03

From the fitting line of the response voltage to position, the change in response voltage can be transferred to the angular shift, and finally the change in refractive index of ordinary light n_o ($n_o = n_s$) by:

$$\frac{\partial n_\gamma}{\partial \theta} = \frac{sin2\theta}{n_\gamma} \approx \frac{\Delta n_\gamma}{\Delta \theta}$$

Table 8 Angular shift of sample 01

Applied voltage (V)	Response voltage (μV)	Angular shift (degree)
3	4.6	0.0000624
6	8.6	0.000117
9	13.9	0.000188
12	17.6	0.000239
15	21.3	0.000289
18	26.6	0.00036

Because of the relationship of the ordinary refractive index change to applied AC voltage:

$$\Delta n_o = -\frac{1}{2} n_o^3 r_{13} \frac{V}{d}$$

the EO coefficient r_{13} can be obtained from the slope of the fitting line:

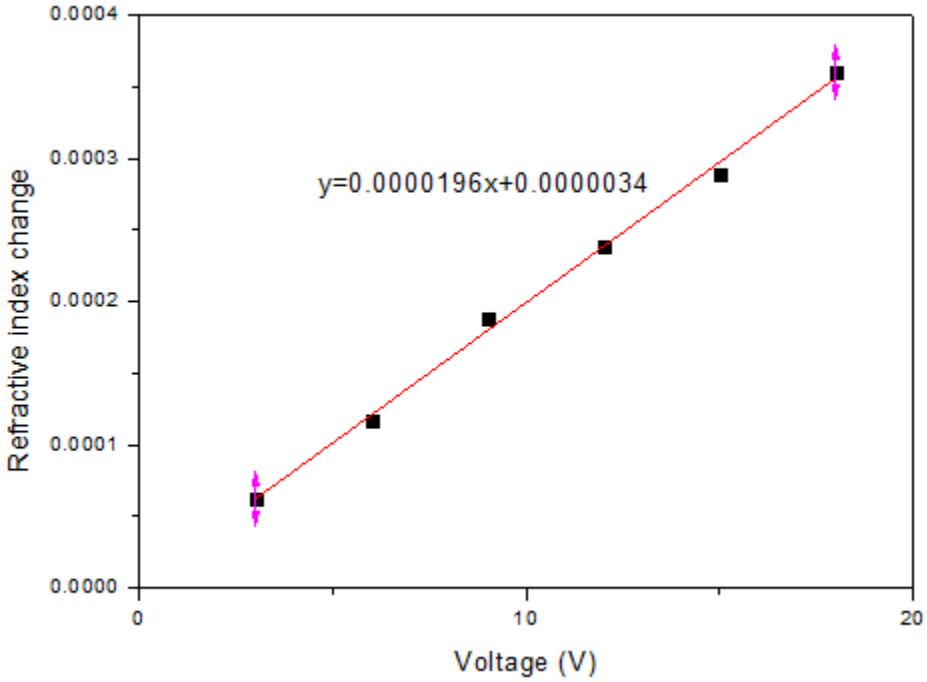

Figure 18 Linear fitting for r13 of sample 01

For the same reason, results of the other two samples can be achieved from the same process and they are listed below:

Table 9 Angular shift of sample 02

Applied voltage (V)	Response voltage (μV)	Angular shift (degree)
6	0.3798	0.000175
9	0.5712	0.000263
12	0.8873	0.000409
15	0.9264	0.000427
18	1.2833	0.000592

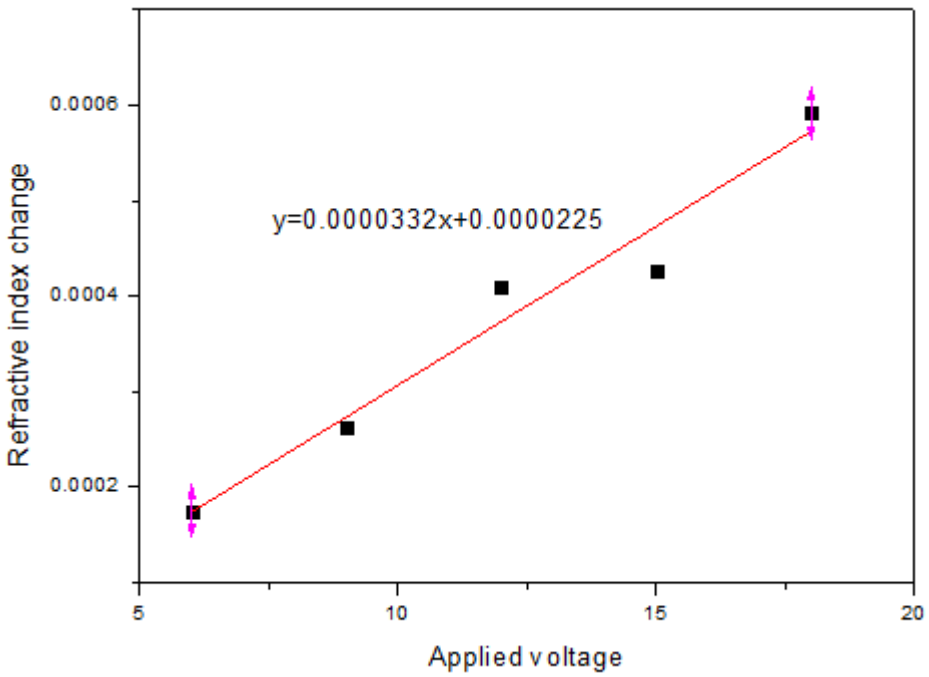

Figure 19 Linear fitting for r13 of sample 02

Table 10 Angular shift of sample 03

Applied voltage (V)	Response voltage (μV)	Angular shift (degree)
3	2.97	0.000146
6	5.15	0.000253
9	7.24	0.000356
12	8.63	0.000424
15	10.88	0.000535
18	13.37	0.000657

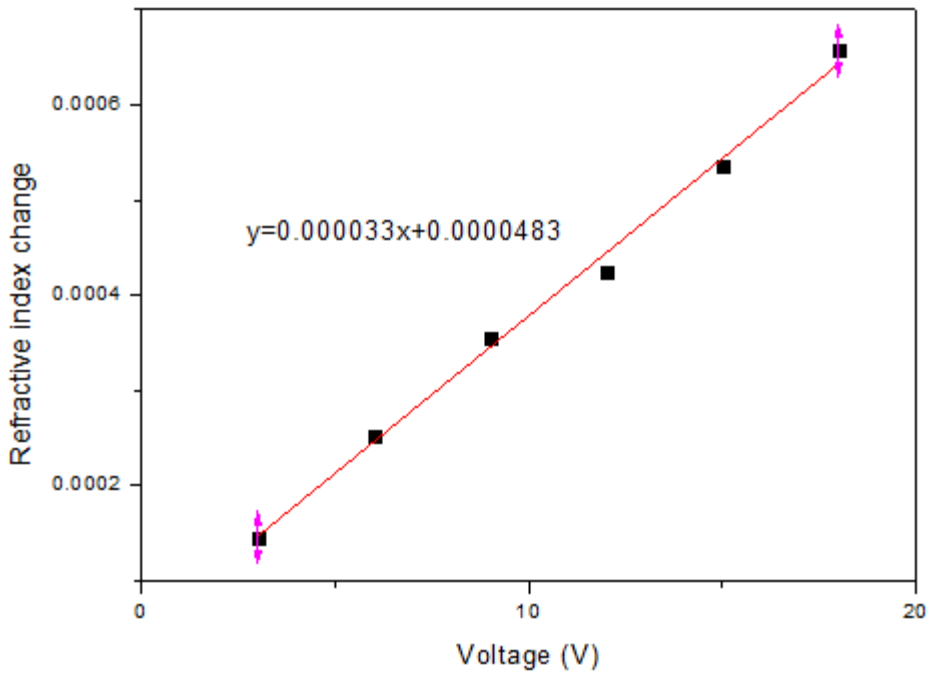

Figure 20 Linear fitting for r13 of sample 03

So the r_{13} of these three samples can be calculated as:

Table 11 Values of r13

Sample	01	02	03	Average
EO coefficient r_{13} (pm/V)	2.064	2.215	2.103	2.127

Calculation for r_{33}

The calculation of the EO coefficient r_{33} is similar in the beginning of the process but different and more complex to get the extraordinary refractive index change Δn_e because the term of Δn_e is related to previous results:

$$\Delta n_e = \frac{n_e^3}{(n_o sin\theta)^2}\left[n_p \Delta n_p + n_o\left(\frac{sin^2\theta}{n_e^2} - 1\right)\Delta n_o\right]$$

From the data of scanning in TM mode, the same starting steps can be taken:

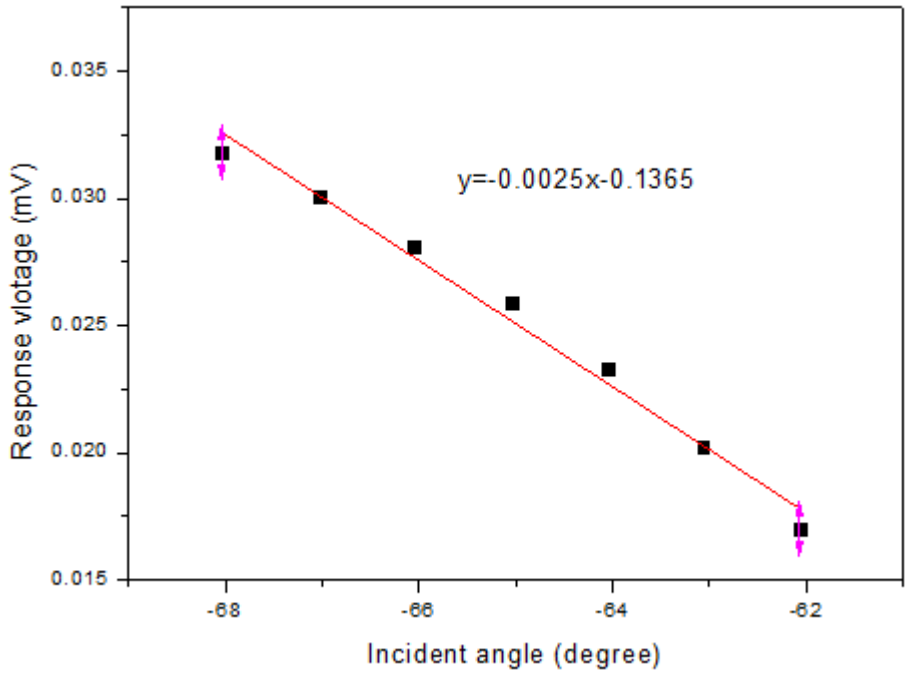

(a)

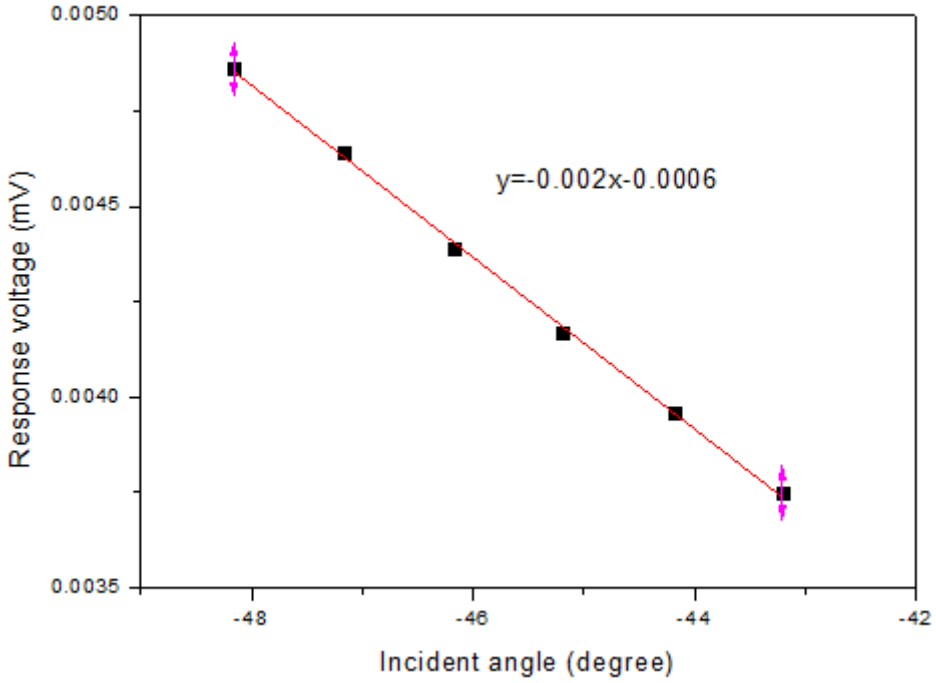

(b)

Figure 21 Linear fitting of TM transmission at half-peak-height (a) sample 02; (b) sample 03

Results of this step can be obtained from the same process. The value of r_{33} comes from the linear relation between the change in extraordinary refractive index and applied voltage:

$$\Delta n_e = -\frac{1}{2} n_e^3 r_{33} \frac{V}{d}$$

Table 12 Angular shift of sample 02

Voltage (V)	Response (μV)	Δn_p	Δn_o	Δn_e
6	0.56	0.000231	0.000175	0.000523
9	0.87	0.000359	0.000263	0.000859
12	1.25	0.000517	0.000409	0.001073
15	1.40	0.000577	0.000427	0.001349

18	1.86	0.000767	0.000592	0.001669

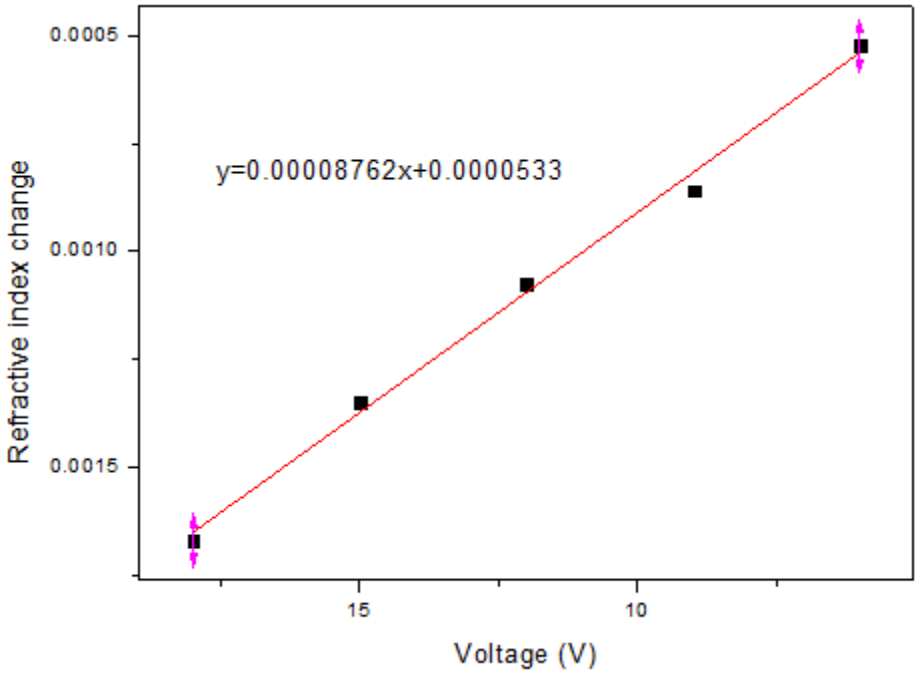

Figure 22 Linear fitting for r33 of sample 02

Table 13 Angular shift of sample 03

Voltage (V)	Response (μV)	Δn_p	Δn_o	Δn_e
6	0.11	0.000295	0.000253	0.000514
9	0.17	0.000478	0.000356	0.001109
12	0.21	0.000591	0.000424	0.001452
15	0.25	0.000703	0.000535	0.001572
18	0.31	0.000872	0.000657	0.001983

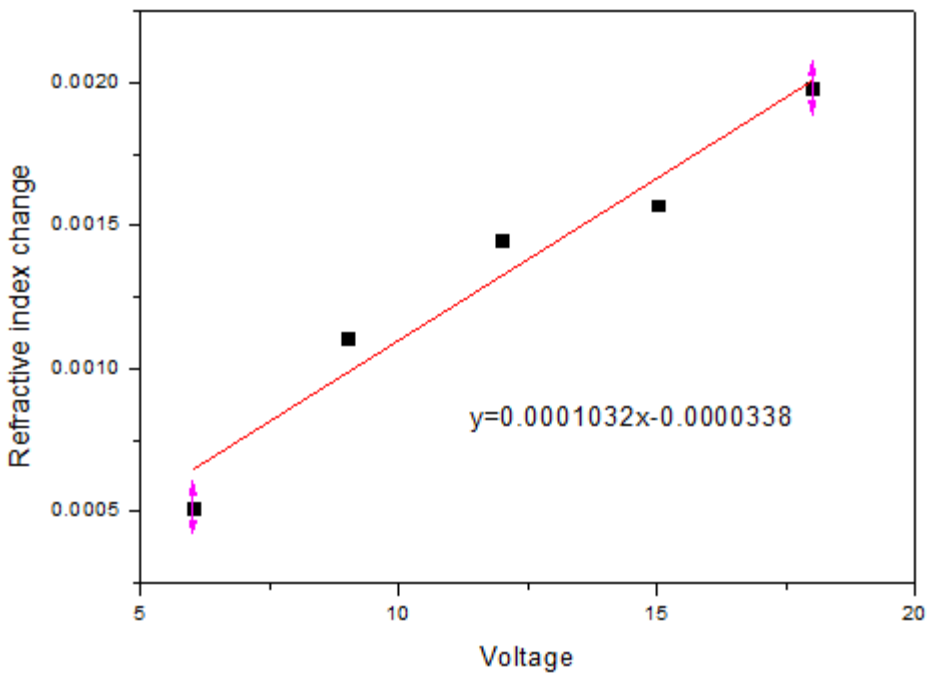

Figure 23 Linear fitting for r33 of sample 03

Table 14 Values of r33

Sample	02	03	Average
EO coefficient r_{33} (pm/V)	5.99	7.07	6.528

By present, results of EO coefficient are 2.127 pm/V for r_{13} and 6.528 pm/V for r_{33}. They are in agreement with the crystal model in which r_{33} should be three times of r_{13} in error beyond 3%.

However, we have only demonstrated the linear relationship between the applied voltage and response. No one can make sure that this response can just come from EO effect without other information. What about the piezoelectric effect in this material? Does the heat produced by weak current change the mechanic properties of this material? Or whether there is one kind of

electromagnetic noise which is also linear to the applied electric field? All these questions will be considered in following research.

C. Greenlee and his co-workers applied the Mach-Zehnder interferometry method to examine EO and piezoelectric effects at the same time[48, 49]. Piezoelectric effect is formed by the electric potential difference at both sides of the film. However, the strength of piezoelectric effect is only determined by the strength of field rather than the direction. As EO effect does not change the original frequency of the signal and it still has the same frequency of the reference signal, piezoelectric effect will produce signal with double frequency. When the sine wave AC signal is applied on the sample, response of piezoelectric effect would be the absolute value of the input signal, shown in the figure below. Although signal with double frequency can also be detected as signal with original frequency, it is difficult for EO signal to be detected at double frequency. So the signal in double frequency is useful for determine the existence of piezoelectric effect.

Analysis and preparation for further study

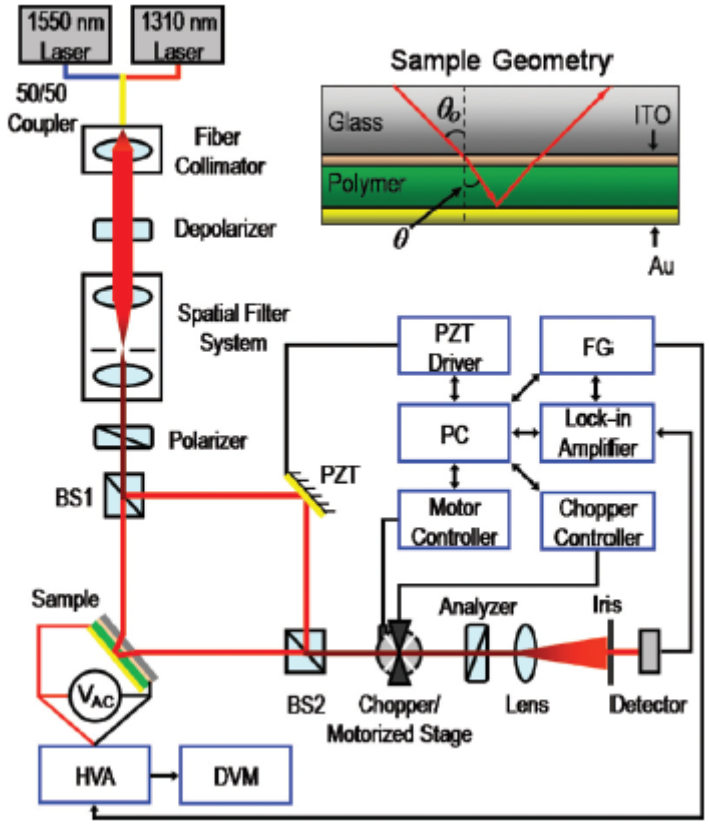

Figure 24 Facility for measurement of piezoelectric effect

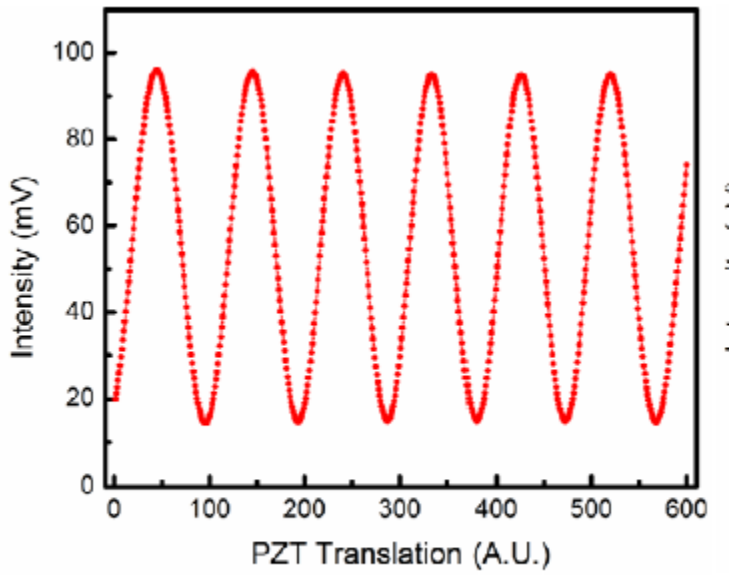

(a)

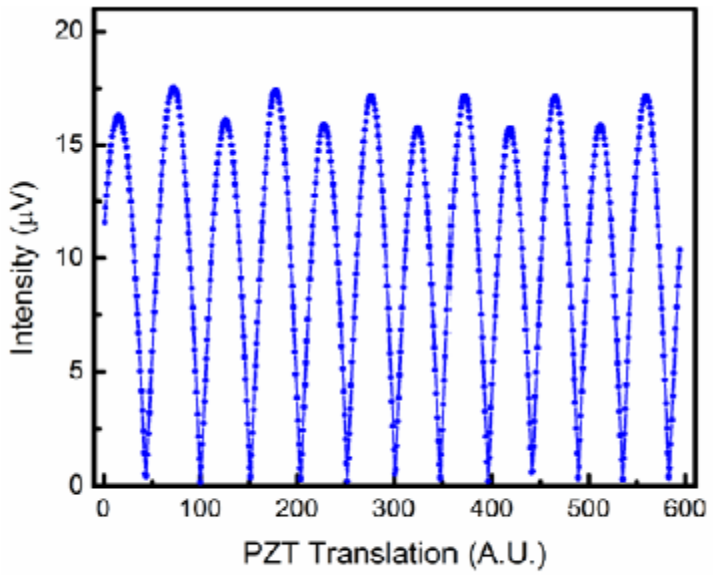

Figure 25 Frequency for signal (a) reference; (b) piezoelectric response

So signal with double frequency of reference signal is examined by lock-in. For each sample, its response voltage in double frequency is always weak and close to the signal without collected signal, which can be considered noise. As a result, piezoelectric effect cannot be a major property of organometal halide perovskite material $MAPbI_3$.

For heat produced by current, it is already known that the change in mechanic properties caused by heat is linear to temperature which is linear to heat. The heat produced by current is linear to the square of voltage ($P = I^2R$ or $P = \frac{U^2}{R}$). So the linear relationship must come from the cooperation of one signal which can offset the effect. There is no such kind of signal already known.

Finally the electromagnetic noise should be analyzed. No matter what it is, the signal of EO effect comes from the laser so if the optical density is modified, the change in collected signal would follow it. Mirrors with different optical density (OD) are put in front of the sample to see

if the change in strength of the incident light would influence the collected signal. The 03 sample is used for this experiment and results are shown below.

Table 15 Response for different transmission

OD	Transmission	Response
0	1	5.15
0.1	0.905	4.52
0.4	0.67	3.45
1	0.368	1.98

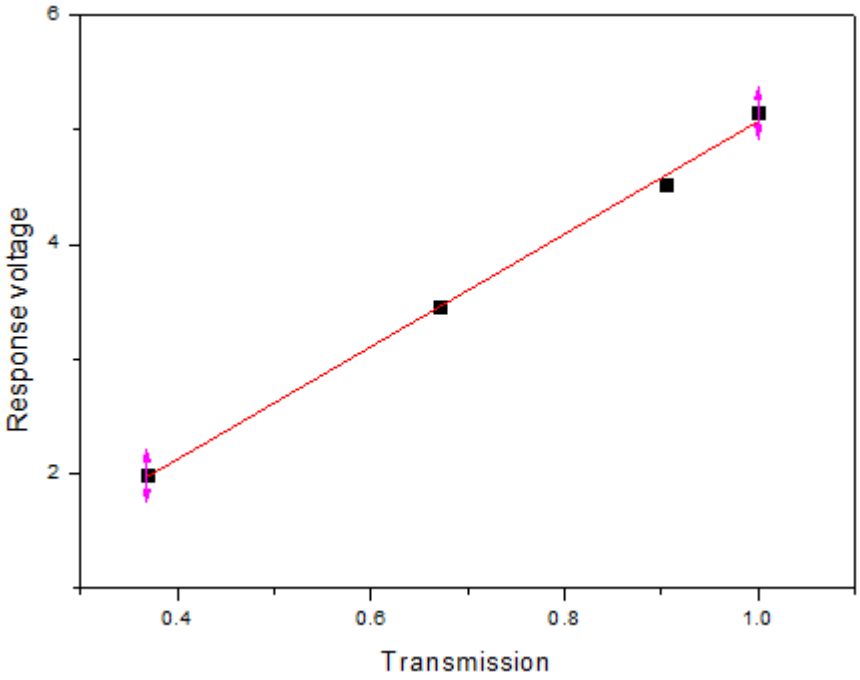

Figure 26 Linear response for transmission

It is obvious that the response voltage is proportional to the transmission of incident light. This is helpful to confirm that the response is from the incident light and it is EO effect.

The results of this project are mainly in technology so it is only a starting step of the study for organometal halide perovskites not only for $MAPbI_3$. Further researches in this direction will pay more attention in the possible cause. The effect from conjugation and polarization for EO effect in organic EO materials have been researched by Larry Dalton and Olbricht BC separately[50,51]. For the chosen organometal halide perovskites materials in this project, $MAPbI_3$, the arrangement of organic cation MA in lattice is different from that of metal cation because the larger volume and different ionic. Compared to metal ion, MA is larger and has an angle between the molecular axis and the direction of electric field. From previous researches, researchers have found that the EO constant is proportional to the acentric order parameter $<\cos^3\theta>$, which is defined by the angle. It means that direct current (DC, or bias voltage) which can change the alignment of ions inside the lattice can lead to different results in response voltage and EO constant. However, it is still not clear what is the model of the EO effect under this case and the role of the alignment of ions. The first step that needs to be figured out is whether there is an existing relation between the alignment of ions and the EO effect. So various bias voltage is applied to the sample in order to see if there is a change in the response voltage and related EO constant.

Table 16 Response and calculated EO constant for different bias voltage

Bias voltage (V)	Response voltage (μV)	EO constant r_{13} (pm/V)
0	6.52	2.1033
2	6.69	2.2045
4	6.86	2.3059

6	7.04	2.4072
8	7.21	2.5086

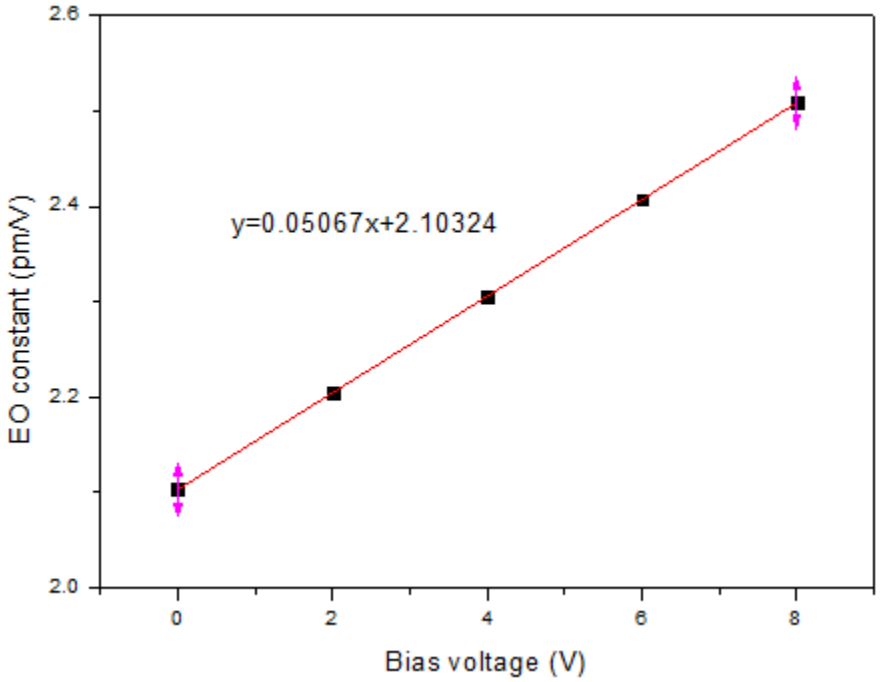

Figure 27 Linear response for bias voltage

Results show that there exists a linear relation between EO constant r_{13} and bias voltage. So the calculated may contain several parts, maybe MA-rotated, non-MA and even the lattice parts. Directions for researches of next step could include the influence of heat on the size of lattice structure, parameters of the rotation and other possible reasons for the observed situation.

Chapter 5: Conclusion and expectation for further study

Organometal halide perovskites film has been made in the middle of a Fabry-Perot interferometer by thermal evaporation of metal poles with masks for special shape and spin-coating for film. By calculating the EO constant, the macroscopic properties of organomatal halide perovskites have been indicated and possible assumption of the theory of this situation in microscopic and molecular scale has been proved.

(1) Details of thermal evaporation for metal poles have been studied by applied profilometer and SEM. From the measured thickness and morphology from SEM images, thickness, uniformity and smoothness of the metal layer under various conditions have been analyzed. Results demonstrate the logarithmic relation of the reflectivity and the thickness of the metal film found in previous researches and confirm the coefficient.

(2) Properties of organometal halide film are researched by XRD, SEM and profilometer. It is found that the film could gain the largest thickness with the best surface morphology at about 2000 rpm in the current recipe.

(3) By putting the organometal halide perovskites film in a Fabry-Perot interferometer between two metal mirrors, the EO constant can be calculated from the transmission data at the position where the transmission is most linear to incident angle for half the height of the peak so that the results can be obtained from the slope of the fitting line with little random error when external electric field is applied to the sample in different voltages. Two important EO constants r_{13} and r_{33} are calculated and used to verify the structure of C_∞ space group of the film from our assumption. Extra measurements are also taken to eliminate the possible results from other causes.

(4) After confirming the linear EO effect in organometal halide perovskites, following researches can pay attention to similar effects in similar composites, the causes of this effect when the change in response voltage for DC bias voltage has been found at the end of this study.

References

1. Muller O, Roy R (1974) The Major Ternary Structure Families, Springer, Berlin Heidelberg New York

2. Wainer E, Soloman S (1942) Titanium Alloy Manufacturing Co. Report 8-9

3. Wul BM, Goldman (1945) Doki Akad. Nauk SSSR 46:154

4. Ogawa, see in Miyake S, Ueda R (1946) J Phys Soc Jpn 1:32

5. Newnham RE, Cross LE (1990) In Kyoui no Chitabari (on $BaTiO_3$) p 325, published by Murata Co. Japan

6. Matthias B, von Hippel A (1948) Phys Rec 73:1378

7. Cross LE, Dennison AT, Nicholson M (1949) Proc Leeds, Phil Soc 5:199

8. Blattner H, Kaenzig W, Merz W (1949) Helv Phys. Acta 22:35

9. Devonshire AF (1949) {hil Mag 40:1040

10. Kay HF, Vousden P (1949) Phil Mag 40:1019

11. D. B. Mitzi, S. Wang, C. A. Field, C. A. Chess, A. M. Guloy, *Science*, 1995, 267, 1473-1476

12. D. B. Mitzi, K. Chondroudis, C. R. Kagan, *IBM J. Res. Dev.*, 2001, 45, 29-45

13. D. B. Mitzi, *J Solid State Chem.*, 1999, 145, 694-704

14. D. B. Mitzi, *Chem. Master*., 1996, 8, 791-800

15. D. B. Mitzi, K. Chondroudis, C. R. Kagan, *Inorg. Chem.*, 1999, 38, 6246-6256

16. A. Kojima, K. Teshima, Y. Shirai, T, Miyasaka, J, Am. Chem. Soc, 2009, 131, 6050-6051

17. H. S. Kim, C. R. Lee, J. H. Im, K. B. Lee, T. Moehl, A. Marchioro, S. J. Moon, R. Humphru-Baker, J. H. Yum, J. E. Moser, M. Gr¨atzel and N. G. Park, *Sci. Rep.,* 2012, 2, 591.

18. M. M. Lee, J. Teuscher, T. Miyasaka, T. N. Murakami and H. J. Snaith, Science, 2012, 338, 643–647.

19. J. Burschka, N. Pellet, S.-J. Moon, R. Humphry-Baker, P. Gao, M. K. Nazeeruddin and M. Gr ätzel, Nature, 2013, 499, 316– 319

20. H. Zhou, Q. Chen, G. Li, S. Luo, T.-b. Song, H.-S. Duan, Z. Hong, J. You, Y. Liu and Y. Yang, Science, 2014, 345, 542–546

21. G. E. Eperon, S. D. Str**anks, C**. Menelaou, M. B. Johnston, L. M. Herz, and H. J. Snaith, Energy Environ. Sci., 2014, 7, 982-988

22. G. Xing, N. Mathews, S. Sun, S. S. Lim, Y. M. Lam, M. Gr ätzel, S. Mhaisalkar and T. C. Sum, Science. 2013, 342, 344-347. 20 Y. J. Fang, Q. F. Dong, Y. C. Shao, Y. B. Yuan and J. S. Huang, *Nat. Photonics*, 2015, DOI: 10.1038/NPHOTON.2015.156

23. Y. J. Yang, Q. F. Dong, Y. C. Shao, Y. B. Yuan, J. S. Huang, *Nat. Photonics*, 2015, DOI: 10.1038/NPHOTON, 2015.156

24. Y. Li, X. Wang, S. Wu, H. Ci, H. Xu, X. Li, H. Sun, Z. Zhang, A. Cao, X. Guo and Y. Li, *J. Mater. Chem. A*, 2015, DOI: 10.1 039/c5ta04936a

25. A. B. Wong, M. Lai, S. W. Eaton, Y. Yu, E. Lin, L. Dou, A. Fu and P. Yang, *Nano Lett*., 2015, 15, 5519-5524

26. A. Fu and P. Yang, *Nat. Mater*., 2015, 14, 557-558

27. Y. B. Yuan, Q. Wang, Y. C. Shao, H.D. Lu, T. Li, A. Gruverman, J. S. Huang, *Adv. Energy Mater*., 2016, 6, 1501803

28. M. J. Yuan, L. N. Quan, R. Comin, G. Walters, R. Sabatini, O. Voznyy, S. Hoogland, Y. B. Zhao, E. M. Beayregard, P. Kanjanaboos, Z. H. Lu, D. H. Kim, E. H. Sargent, *Nat. Nanotech.*, 2016, DOI:10.1038/NNANO.2016.110

29. Z. G. Xiao, R. A. Kerner, L. F. Zhao, N. L. Tran, K. M. Lee, T. W. Koh, G. D. Scholes, B. P. Rand, *Nat. Photonics*, 2017, DOI:10.1038/NPHOTON.2016.269

30. Y. H. Kim, H. Cho, J. H. Heo, T. S. Kim, N. S. Myoung, C. L. Lee, S. H. Im and T. W. Lee, *Adv. Mater*., 2015, 27, 1248-1254

31. L. Dou, Y. Yang, J. You, Z. Hong, W. H. Chang, G. Li and Y. Yang, *Nat. Commun*., 2014, DOI: 10.1038/ncomms6404

32. H. M. Zhu, Y. P. Fu, F. Meng, X. X. Wu, Z. Z. Gong, Q. Ding, M. V. Gustafsson M.T. Trinh, Song Jin and X-Y. Zhu, *Nat Mater.*, 2015, 14, 636-643

33. N. Ahn, D. Y. Son, I. H. Jang, S. M. Kang, M. Choi, N. G. Park, *J. Am. Chem. Soc.*, 2015, 137, 8696-8699

34. J. Domaradzki, D. Kaczmarek, M. Mazur, D. Wojcieszak, J. Halarewicz, S. Glodek, P. Domanowski, *Mater. Sci.-Poland*, 2016, DOI: 10.1015/msp-2016-0102

35. J. W. Lee, D. H. Kim, H. S. Kim, S. W. Seo, S. M. Cho, N. G. Park, *Adv. Energy Mater.*, 2015, 5, 1501310

36. M. Saliba, S. Orlandi, T. Matsui, S. Aghazada, M. Cavazzini, J. P. C. Baena, P. Gao, R. Scopelliti, E. Mosconi, K. H. Dahmen, F. D. Angelis, A. Abate, A. Hagfeldt, G. Pozzi, M. Graetzel, M. K. Nazeeruddin, *Nat. Energy*, 2016, DOI: 10.1038/NENERGY.2015.17

37. J. P. C. Baena, A. Abate, M. Saliba, W. Tress, T. J. Jacobsson, M. Gratzel, A. Hagfeldt, *Energy Environ. Sci.*, 2017, 10, 710

38. D. Y. Son, J. W. Lee, Y. J. Choi, I. H. Jang, S. Lee, P. J. Yoo, H. Shin, N. Ahn, M. Choi, D. Kim, N. G. Park, *Nat. Energy*, 2016, DOI: 10.1038/NENERGY.2016.81

39. N. G. Park, M. Gratzel, T. Miyasaka, K. Zhu, K. Emery, *Nat. Energy*, 2016, DOI: 10.1038/NENERGY.2016.152

40. P. Ramasamy, D. H. Lim, B. Kim, S. H. Lee, M. S. Lee, J. S. Lee, *Chem. Commun.*, 2016. 52. 2067

41. J. W. Lee, H. S. Kim, N. G. Park, *Chem. Res.*, 2016, 49, 311-319

42. N. Sahu, B. Parija, S. Panigrahi, *Indian J. Phys.*, 83(4) 493-452 (2009)

43. Teng, C.C.; Man, H.T., *Appl. Phys. Lett*.1990, 56, 1734-1736

44. Schildkraut, J.S., *App. Opt.* 1990, 29, 2839-2841

45. Park, D.H.; Lee, C.H.; Herman, W.N., *Opt. Express* 2006, 14, 8866-8884

46. D. H. Park, J. D. Luo, A. K.-Y. Jen, W. N. Herman, *Polymers* 2011, 3, 1310-1324

47. Yeh, P. *Optical Waves in Layered Media*; John Wiley & Sons: Hoboken, NJ, USA, 1988

48. C. Greenlee, A. Guilmo, A. Opadeyi, R. Himmelhuber, R. A. Norwood, M. Fallahi, J. D. Luo, S. Huang, X. H. Zhou, A. K.-Y. Jen, N. Peyghamberian, *Appl. Phys. Lett.* 97, 041109 (2010)

49. C. Greenlee, A. Guilmo, A. Opadeyi, R. himmelhuber, R. A. Norwood, *Proc. of SPIE Vol.* 7774 77740D-8

50. L. Dalton, S. Benight, *Polymers* 2011, 3, 1325-1351

51. B. C. Olbricht, P. A. Sullivan, P. C. Dennis, Jeffrey T. Hurst, L. E. Johnson, S. J. Benight, J. A. Davies, A. Chen, B. E. Eichinger, P. J. Reid, L. R. Dalton, B. H. Robinson, *J. Phys. Chem. B* 2011, 115, 231-241